UiT The Arctic University of Norway

Faculty of Science and Technology
Department of Chemistry

Effects of single and multiple OXA-48 mutants on enzyme activity, stability, and structure-activity relationship

Evolutionary consequences of antibiotic resistance development caused by OXA-48

Nina Nevjar Martinsen

KJE-3907, Mastergradsoppgave i kjemi ved lektorutdanningen trinn 8 - 13 – May 2022, 40 ECTS

Acknowledgments

Table of Contents

Contributions

	Contributors
Protein purification	Christopher Fröhlich
Enzyme kinetics	Nina Nevjar Martinsen Christopher Fröhlich
Differential scanning fluorimetry	Nina Nevjar Martinsen
Protein crystallization	Nina Nevjar Martinsen
X-ray crystallography data collection and structure refinement	Christopher Fröhlich Hanna-Kirsti S. Leiros
Structure analysis	Nina Nevjar Martinsen

Abbreviations

$\Delta\varepsilon$:	Extinction coefficient
BIS-TRIS propane:	1,3-bis[tris(hydroxymethyl)methylamino]propane
Da:	Dalton
DBL:	Class D β-lactamase
DSF:	Differential scanning fluorimetry
ESRF:	European Synchrotron Radiation Facility
E. coli	*Escherichia coli*
OD:	Optical density
HEPES:	4-(2-Hydroxyethyl)-1-piperazine ethanesulfonic acid
k_{cat}:	Turnover number in Michaelis-Menten kinetics
K_m:	Dissociation constant for enzyme-substrate complex in Michaelis-Menten kinetics
K. pneumoniae:	*Klebsiella pneumoniae*
OXA	Oxacillinase
OXA-48:Q5:	OXA-48:A33V/K51E/F72L/S212A/T213A
PBP:	Penicillin binding protein
PEG MME:	Polyethylene glycol monomethyl ether
SBL:	Serine-β-lactamase
T_m:	Transition midpoint temperature
wt:	wild type
Å:	Ångstrom

Abstract

Antimicrobial resistance, primarily caused by the overuse of antimicrobials such as antibiotics, is becoming an increasing concern to public health. To that end, the global spread of the β-lactamase OXA-48 is worrisome, as it readily catalyzes the hydrolysis of β-lactam drugs, such as penicillins as well as our "last resort" carbapenems. On the contrary, OXA-48 exhibits only limited catalytic activity against 3rd generations cephalosporins like ceftazidime. However, naturally evolving variants and results from laboratory studies have shown that OXA-48 can expand its substrate profile, conferring increased ceftazidime resistance. Expansion of the substrate profile towards ceftazidime is seen to be accompanied by a trade-off towards carbapenems and penicillins, greatly reducing OXA-48 ability to catalyze the hydrolysis of penicillins and carbapenems. Here, X-ray crystallography, steady-state enzyme kinetics and differential scanning fluorimetry were used to characterize and analyze wild type (wt) OXA-48:wt and two variants, OXA-48:F72L and OXA-48:A33V/K51E/F72L/S212A/T213A (OXA-48:Q5), where the latter two were evolved towards increased ceftazidime resistance. Steady-state enzyme kinetics revealed that the two mutants had increased catalytic ability to hydrolyze ceftazidime. Such increases in k_{cat}/K_m hypothesized to arise from increased flexibility of the Ω-loop, which was observed in the OXA-48:Q5 X-ray crystal structure in complex with piperacillin, is in line with previous studies. Further supporting the hypothesis, urea dependent kinetics and thermostability measurements show that these mutants likely exhibit increased dynamical behavior that would aid ceftazidime binding. OXA-48:F72L showed a bigger urea dependence on the enzyme activity with no activity at 4 M urea, whereas OXA-48:wt and OXA-48:Q5 needed 6 M urea to become inactive. This suggested that OXA-48:F72L is more flexible, and that OXA-48:Q5 regains some resistance to chemical denaturing by urea. The pH dependency showed higher piperacillin activity at pH 7.2 compared to 5.2 and 9.2 for all three variants. The increase in ceftazidime activity came along with a functional trade-off against the penicillin piperacillin as well as reduced thermostability of (OXA-48:F72L: -6.5°C/OXA-48:Q5: -6.4°C) compared to wt OXA-48, which may be caused by sub-optimal substrate positioning within the active site of OXA-48:Q5. This work provides experimental evidence, that during evolution of OXA-48 towards increased ceftazidime activity, structural changes can arise, likely affecting the chemical environment within the active site, causing increased enzyme flexibility, and ultimately shaping functional trade-offs.

Aims of study

The aims of this study were to investigate changes within the previously evolved single mutation OXA-48:F72L and the variant OXA-48:Q5 evolved towards increased ceftazidime. A goal of the work was to investigate the catalytic relevance of laboratory acquired mutations and if they consequently increase cephalosporinase activity within OXA-48, in addition to studying if any changes in penicillinase activity of the evolved mutants could be observed. Additional goals included understanding functional trade-offs within the variants evolved towards ceftazidime resistance, and to investigate if X-ray crystallography of a the OXA-48:Q5 mutant structure in complex with piperacillin could shed light on functional trade-offs, such as changes in activity, thermostability, pH dependence, the effect from denaturing conditions with urea, and intramolecular interactions.

1 Introduction

Antimicrobial resistance, which is primarily caused by the overuse of antimicrobials such as antibiotics, is becoming an increasing concern to public health. The World Health Organization has recognized antimicrobial resistance as "a global health security threat that requires action across government sectors and society as a whole." [1]. It is anticipated that by 2050, the number of fatalities caused by antimicrobial resistance will have risen to 10 million deaths per year, unless action is made to limit the use of antimicrobials and discover new inhibitors or new antimicrobials [2]. Antimicrobial resistance has been observed since the discovery of antibiotics, although the process has been accelerated by the widespread use of antibiotics [3, 4]. Among the β-lactamase enzymes oxacillinases (OXAs) are a great concern, due to their rapid spread throughout the world, and their tendency to acquire amino acid substitutions leading to various phenotypic variants [5]. OXAs are class D β-lactamases, which have the capacity to hydrolyze and inactivate carbapenem type β-lactams, which are regarded as a last resort drug [6]. OXA-48 exhibits only limited catalytic activity against 3rd generations cephalosporins like ceftazidime [7]. However, naturally evolving variants and results from laboratory studies have shown that OXA-48 can expand its substrate profile [8]. Expansion of the substrate profile towards ceftazidime is seen to be accompanied by a trade-off towards carbapenems and penicillins, greatly reducing OXA-48 ability to catalyze the hydrolysis of penicillins and carbapenems [9, 10]. It is speculated that this trade-off appears due to the large molecular size of ceftazidime, and a widening of the active site that causes other lactams to bind less efficiently. The emerge of new β-lactamase inhibitors in one encouraging perspective in the fight against antibiotic resistance [3]. Studying the structure and mechanisms driving resistance are important to develop new inhibitors and sustainable use of the current antibiotics. Being able to understand functional trade-offs on both phenotypic and structural level of enzymes therefore addresses important medical and evolutionary questions.

1.1 β-lactam antibiotics

β-lactams antibiotics are the most widespread group of antibacterials and account for 50% of the commercially available antibiotics used worldwide [3, 11]. The β-lactam antibiotics all contain a four-membered ring and can be divided into four clinically relevant classes based on their structure which include penicillins, cephalosporins, carbapenems and monobactams, whose core structures can be seen in Figure 1A. Penicillins are five-membered and only contain one site for different sidechains, compared to the other classes which all have two R-groups in their structure giving them a wider structural diversity than penicillins [11]. Carbapenems contains a five membered ring and cephalosporins contains a six-membered ring fused to the β-lactam core. Monobactams differ from the other classes as they do not possess a ring structure fused to the β-lactam core and they are predominantly synthetically made [11, 12].

β-lactam antibiotics target the cross-linked peptidoglycan layer, or the cell wall of bacteria, inhibiting the synthesis of this layer, resulting in a weakening of the cell wall in both Gram-negative and Gram-positive bacteria. β-lactams form covalent bonds with the bacterial essential penicillin-binding proteins (PBPs) that are involved in the terminal steps of the cross-linking of the peptidoglycan layer. This mechanism is possible due to the β-lactams being a substrate analogue of the two D-alanine residues, the natural substrate of the PBPs [11]. Bacteria heavily rely on the cell wall and weakening the cell wall makes the bacteria susceptible to cell lysis and ultimately cell death [3, 13]. In the following section two relevant β-lactams antibiotics will be presented.
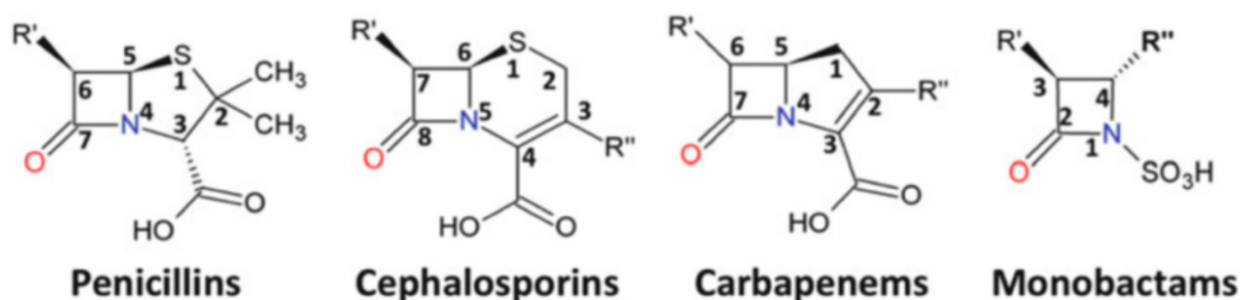
Figure 1A: Core structures of the β-lactam antibiotic classes penicillins, cephalosporins, carbapenems and monobactams. Figure reprinted with permission from [11].

1.1.1 Piperacillin

Piperacillin is a 4th generation extended spectrum ureidopenicillin β-lactam antibiotic derived from ampicillin with increased activity against gram-negative bacteria, especially used towards *P. aeruginosa* infections [14]. Piperacillin was approved for clinical use in 1981 and is still in use today, and is a part of the class penicillins, which was the first β-lactam class to be used clinically[3, 15]. The structure of piperacillin can be seen in Figure 1B. Penicillins are still an important part of the clinical antibiotics, but is subject to widespread resistance due to the overuse of the drug [3].

1.1.2 Ceftazidime

Clinical development of cephalosporins stemmed from their resistance to hydrolysis by penicillinases and are generally grouped into four generations based on their activity. Unlike penicillins, cephalosporins have two R-groups, which give rise to structural diversity within the class[11]. Ceftazidime is a 3rd generation oxyimino-cephalosporin that was approved for clinical use in 1985, and the structure can be seen in Figure 1B. Third generation cephalosporins have continuously served as important antibiotics for treatment of infections caused by Gram-negative pathogens, and ceftazidime maintains its observed activity against *P. aeruginosa* [3].
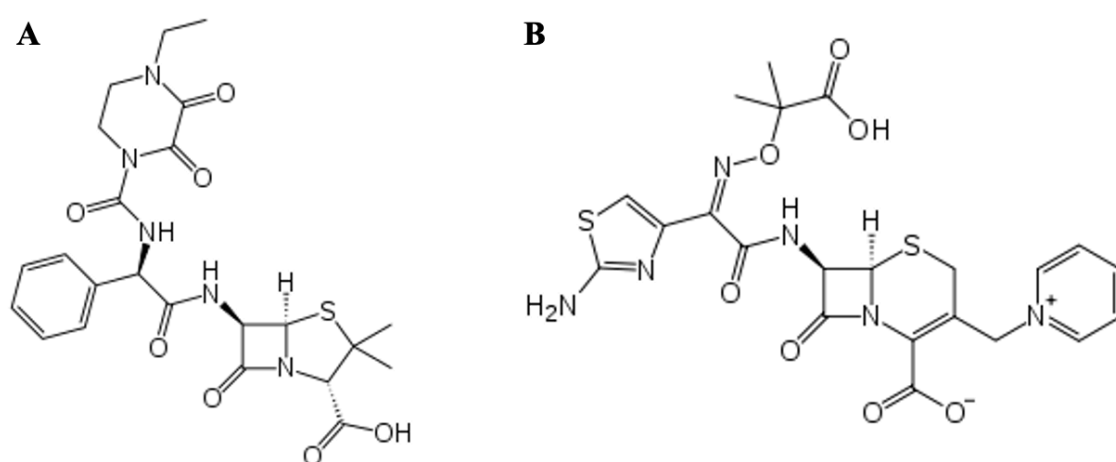
Figure 1B: The molecular structure of A) piperacillin and B) ceftazidime.

1.2 Antibiotic resistance, the β-lactamase enzymes and OXA-48

Bacteria have developed resistance mechanisms conferring resistance to all classes of β-lactam antibiotics. In fact, resistance to β-lactams has been shown to represent a driving role in infections caused by antibiotic-resistant bacteria. There are three major mechanisms involved in resistance development: regulation of β-lactam entry and efflux, altering the binding site of the antibiotics and inactivation of the antibiotic [11, 13]. In Gram-negative bacteria, the production of β-lactamase enzymes represents one of the most prevalent β-lactam resistance mechanisms, namely the inactivation of the antibiotic [16]. These enzymes catalyze the hydrolysis of the β-lactams four-membered ring, rendering the β-lactam biologically inactive. An example of this can be seen in Figure 1C, with the β-lactam penicillin used as an example.

β-lactamases can be classified either by their structure, using the Ambler classification system, or according to their function, using the Bush-Jacoby system [16]. The Ambler classification system groups β-lactamases into four classes; A, B, C and D. While class B are metallo-β-lactamases (MBLs) which utilize zinc ions for β-lactam hydrolysis, other Ambler classes such as A, C and D are serine-β-lactamases (SBLs), enabling an active site serine for β-lactam hydrolysis. Bush and Jacoby groups the enzymes in three main classes based on their functional groups, with subclasses based on their inhibitor and substrate profiles [16, 17].
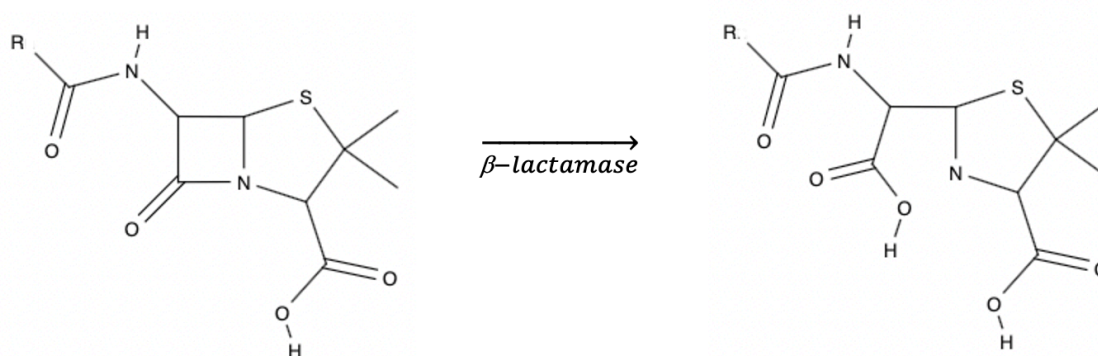
Figure 1C: The hydrolysis of penicillin from active penicillin to inactivated penicillin, performed by a β-lactamase enzyme.

Class D β-lactamases are also known as the oxillinases (OXA) enzymes, named after their ability to hydrolyze the penicillin oxacillin [11].These enzymes have evolved the ability to hydrolyze carbapenems and oxyimino-cephalosporins have given the enzymes a cause for concern [18]. OXA-48 was first identified in Turkey in 2001, in a *K. pneumoniae* strain resistant to all β-lactams [19]. OXA-48 catalyzes the hydrolysis of penicillins efficiently but exhibits only promiscuous activity against 3rd generations cephalosporins like ceftazidime [7]. OXA-48 has been reported with catalytic efficiencies towards penicillins like oxacillin and ampicillin of 10^6 $M^{-1}s^{-1}$, and a catalytic efficiency towards the cephalosporin ceftazidime reported as low as 1 $mM^{-1}s^{-1}$ [18, 19]. However, naturally evolving variants and results from laboratory studies have shown that OXA-48 can expand its substrate profile, and the enzyme has gained attention due to its large clinical prevalence and broad specificity [8, 20]. Previous studies of variants with increased resistance against the substrate ceftazidime revealed expansion of the substrate profile, that was accompanied by functional trade-offs towards penicillins and carbapenems [5, 9].

Class D serine-β-lactamases like OXA-48 have been observed to have hydrophobic regions in the active site that favors the carboxylation of K73 by decreasing the pK_a value of the sidechain, which allows carboxylated K73 to be stabilized by surrounding residues and exist at a neutral pH [11, 21, 22]. Figure 1D shows the hydrolysis mechanism of OXA-48 for a general carbapenem substrate, which includes acylation (step 1-3) and deacylation (step 4-6). The first step is acylation and the formation of a non-covalent complex between β-lactam and the β-lactamase. Carboxylated K73 acts as a general base by deprotonating S70, which is the active site serine, and in return increases its nucleophilicity. The deprotonated S70 can then attack the carbonyl of the β-lactam ring, resulting in a covalent acyl-enzyme complex (step 3). The deacylation requires an activated water molecule to be present in the active site to attack the acyl-enzyme structure (step 4), cleaving the final hydrolysis product (step 6) off the enzyme [23].
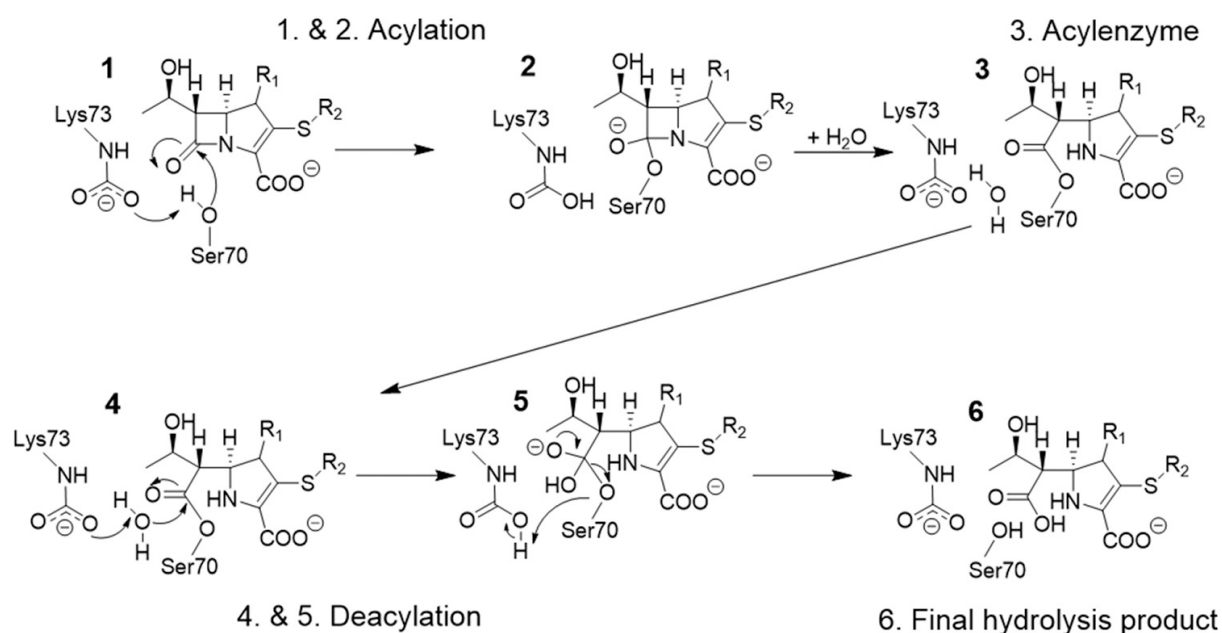
Figure 1D: Shows the mechanism with acylation (step 1-3) and deacylation (step 4-6) of OXA-48. Reused with permission from [23].

1.3 Enzymatic properties, structure, and stability studies

1.3.1 Enzyme kinetics

Enzymes are highly specific biological catalysts that speed up the rate of a chemical reaction without becoming permanently altered in the process [24]. Enzymes cannot alter the equilibrium between reactants and product, only increase the rate of attainment of that equilibrium by lowering the activation energy [25]. Many biological reactions such as the hydrolysis of β-lactams occur spontaneously, but can have degradation half-lives of several days, but in the presence of an enzyme the reaction rate can be accelerated to occur in only seconds [26, 27].

Enzyme kinetics is used to study the rates of enzyme-catalyzed reactions such as the catalytic efficiency, catalytic constants, binding affinity, and the maximum velocity of the reaction. These rates can help us understand the evolution of enzymes or design enzymes with increased catalytic abilities, which can be useful in drug discovery and design [28]. Synonymous to enzymology and enzyme kinetics is the Michaelis-Menten model, which relates the substrate concentration [S] to velocity [29].

The model describes how the enzyme-catalyzed reaction involve the conversion of substrate to product. The reaction mechanism for the hydrolysis of β-lactams by β-lactamases is depicted schematically in Equation 1 and include formation of non-covalent enzyme-substrate complex (ES), the formation of an acyl-enzyme intermediate (ES*) and hydrolysis of the product. In the equation E is free enzyme, S is the substrate and P is product.

Equation 1
$$E + S \underset{k_{-1}}{\overset{k_1}{\rightleftharpoons}} ES \overset{k_2}{\rightarrow} ES^* \overset{k_3}{\rightarrow} E + P$$
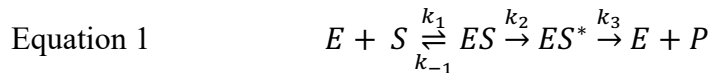
The equation also includes rate constants, where k_1 is the rate of formation of the non-covalent enzyme-substrate complex ES and k_{-1} is the backwards reaction. k_2 is the rate of formation of the acyl-enzyme intermediate, and k_3 is the deacylation[30].

The model assumes that the formation of product is irreversible, so that the reverse reaction of k_3 is negligible. It also assumes that there is a much greater amount of substrate than enzyme, so that even when all the enzyme is bound in an enzyme-substrate complex, there is still excess substrate. In addition, the Michaelis-Menten model is based on the steady state assumption, where the rate of breakdown of the enzyme-substrate complex is equal to the rate of formation of the enzyme-substrate complex. With these assumptions an enzyme-catalyzed reaction which only binds to one substrate can be described by the Michaelis-Menten equation shown in Equation 2 [29, 31].

Equation 2
$$v = \frac{V_{max}[S]}{K_m + [S]}$$

In this equation v is the velocity, v_{max} is maximum velocity when all the enzyme is complexed to the substrate and [S] is substrate concentration, which can be plotted as a Michaelis-Menten curve seen in Figure 1E. K_m is referred to as the Michaelis-Menten constant and is equal to the substrate concentration that results in half-maximum velocity for the reaction. This constant can be used as relative measure of the enzymes binding affinity to the substrate.

k_{cat}, or the turnover number of the enzyme defines the number of catalytic turnover events that occur per unit time, and reflects the relationship between the acylation and deacylation rate constants[30]. Dividing k_{cat}/K_m gives the enzymes catalytic efficiency and is useful for comparing the activity of enzymes, where most enzymes have catalytic efficiencies, k_{cat}/K_m values, of 10^5 - 10^8 $M^{-1}s^{-1}$ for their native substrates [29, 32].
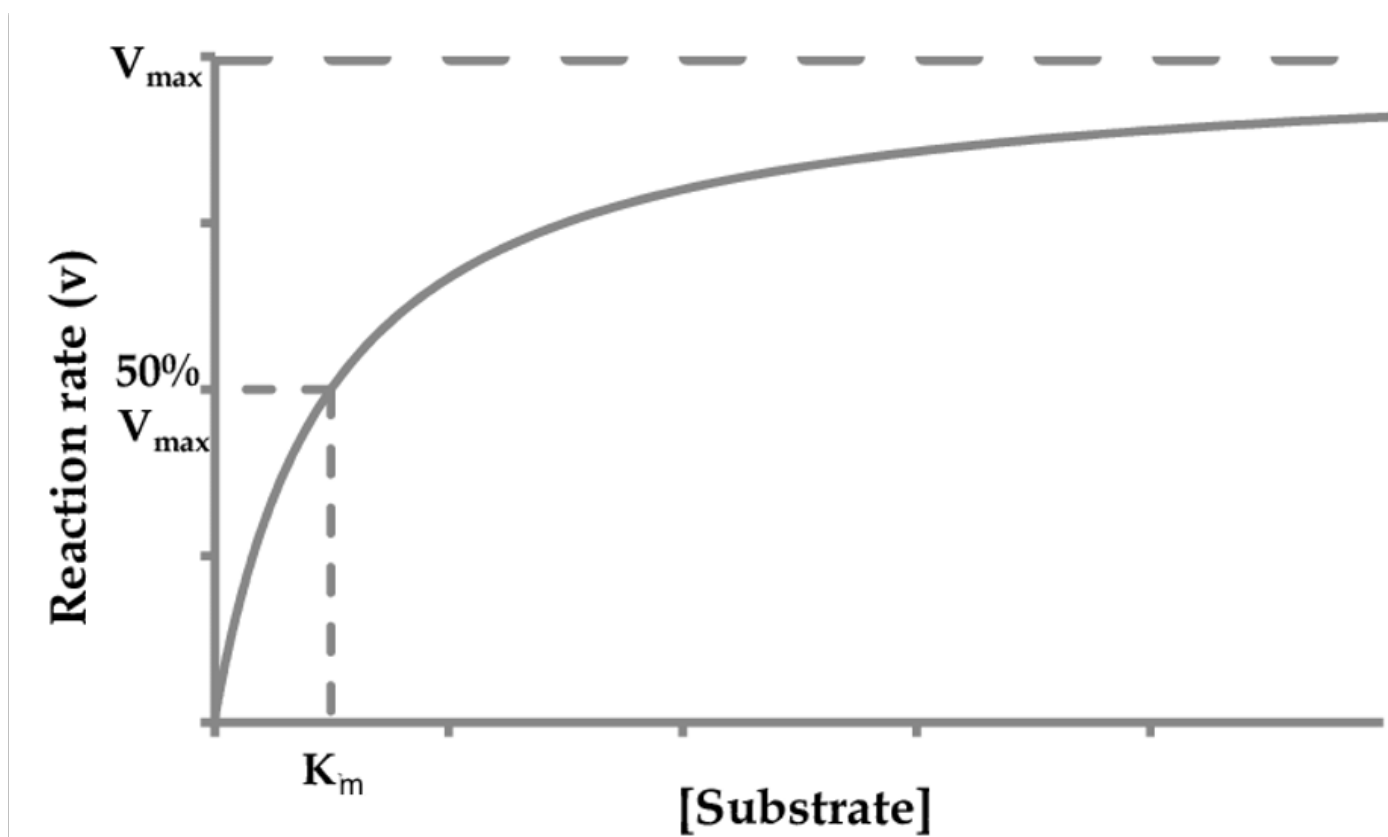
Figure 1E: Michaelis-Menten kinetics curve shows a plot of reaction rate (v) as a function of substrate concentration. v_{max} is the maximum velocity of the particular enzyme, K_m, or the Michaelis-Menten constant, is the substrate concentration that results in half-maximal velocity for the enzyme-catalyzed reaction. Figure from reference [33].

1.3.2 Differential scanning fluorimetry

Differential scanning fluorimetry (DSF), uses a fluorescent dye to measure protein unfolding. A fluorescent dye (such as SYPRO orange) binds to the hydrophobic regions of the protein, which gets exposed when the protein unfolds by thermal induction, shown in Figure 1F as a schematic representation of the process [34]. When the protein gets subjected to gradually increasing temperature, and the change in fluorescence intensity as a function of temperature can be utilized to determine the proteins melting temperature (T_m) [35]. DSF is also known as protein thermal shift assay, as it can be used to add stabilizing or destabilizing components to the solution to observe any shift in the proteins melting temperature upon additions [36]. The melting temperature, or the transition midpoint, obtained using DSF is calculated from the first derivative of the melting curve, and this value is defined as the temperature at which the concentration of folded and unfolded protein are both 50% [36, 37].
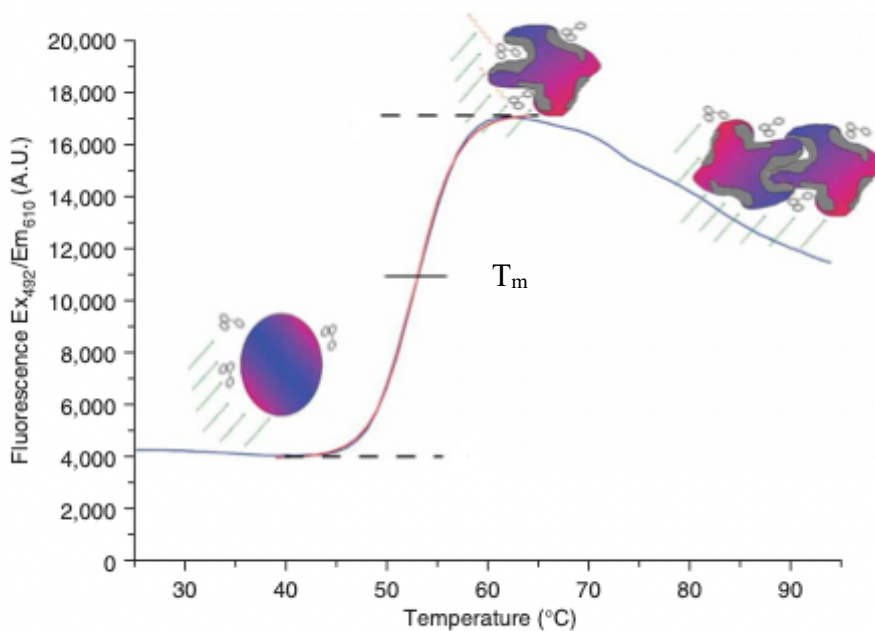
Figure 1F: Shows the globular protein (pink and purple) which emits a basic fluorescence intensity at 492 nm (green curved arrows). As the protein unfolds hydrophobic regions of the protein (grey) becomes exposed and dye molecules bind to these regions. A strong fluorescent light at 610 nm is emitted (orange curved arrows) from the dye. As the peak is reached, a gradual decrease is observed as the protein aggregates and precipitates. T_m shows the transition midpoint of the curve. Adapted with permission from [36].

1.3.3 Protein crystallization and X-ray crystallography

X-ray crystallography is by far the most utilized method to determine the structure of macromolecules such as proteins [38]. As of April 2022 structures solved by X-ray crystallography made up 86.9% of the structures in the Protein Data Bank atomically resolved 3D structures of biologically active molecules can be used for identifying binding sites, understanding the origin of dynamics and stability properties, protein engineering and modern drug and vaccine design to name a few [39]. The ultimate goal of protein X-ray crystallography is to obtain a high resolution three-dimensional electron density map of the protein in the crystal, which can be interpreted to build an atomic model [40]. These maps show the average structure of the molecules in the crystal. Even though the structures obtained requires human intervention to interpret, often aided by computer programs, the electron density maps is an objective result from a productive crystallographic experiment [26].

Successfully obtaining crystals of sufficient quality and size is often the rate-limiting step in structure determination using X-ray crystallography [26, 41, 42]. Crystallizing proteins have no universal methodology as the parameters can be widely different between different enzymes. A trial-and-error approach is used for searching for ranges of parameters that influence the formation of crystals until some crystals form, and finally optimizing those conditions to yields higher quality crystals. Commercial screens can be utilized to search a wide range of parameters when working with a new protein. Screening for the right conditions to grow protein crystals such as changing the pH, concentration, temperature, and precipitant type requires a great amount of protein, though the use of crystallization robots can limit the protein usage some. Protein crystallization can be described by the phase diagram in Figure 1G which shows different zones of the phases the protein can reach during crystallization. Crystallization requires a supersaturated state, a non-equilibrium condition where the protein concentration is above the solubility limit. From the supersaturated state equilibrium can be established by formation of a solid state, such as a stable nucleus of a crystal, which can then grow until the system regains equilibrium. If a crystal does not grow, the protein can precipitate out of the solution for the system to regain equilibrium [41].
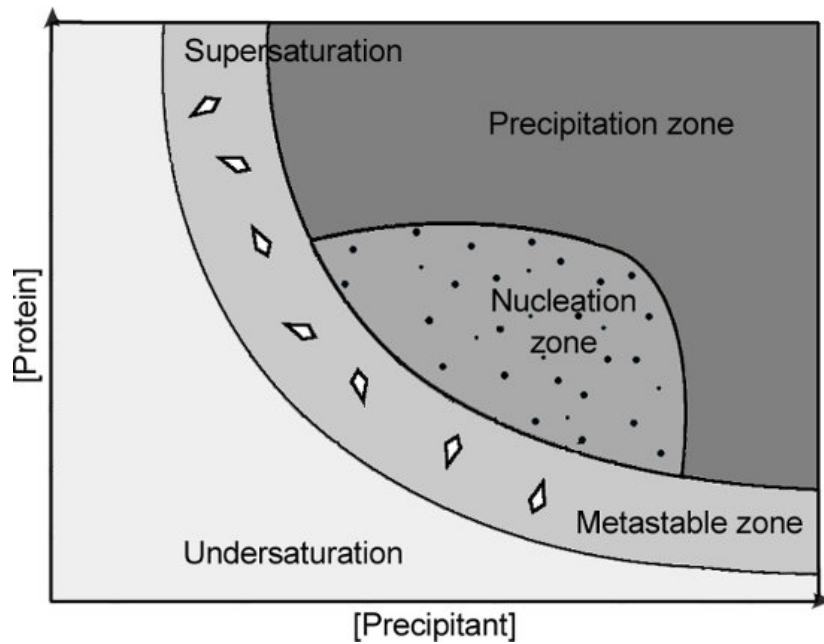
Figure 1G: Phase diagram for crystallization of proteins. It is divided by the solubility curve into under- and supersaturated zones, and in the undersaturated zone the protein will not crystallize. In the metastable zone spontaneous nucleation will not occur unless induced by introducing a particle or vibration. In the nucleation zone crystals can form spontaneously. In the precipitation zone insoluble protein separates from the solution into an amorphous state, which occurs at very high supersaturation [43]. Supersaturation is a phase with a non-equilibrium condition where protein concentration is above the solubility limit. To re-establish equilibrium a solid state, like crystals, can form. To reach a supersaturated solution to promote formation of a solid state, the properties of the solution must be modified [41]. Figure from [44].

Vapor diffusion is a common technique used for crystallizing proteins and is done by placing a drop containing a mixture of protein solution and precipitation agent in a sealed chamber containing precipitation agent. The water inside of the drop slowly diffuses out until the osmolarity of the well content and the drop is equal, which will cause dehydration of the drop, ideally supersaturating the protein in the metastable zone [41, 45]. Vapor diffusion can be performed using either a hanging drop method (the drop hangs above the reservoir solution on a cover slit), sitting drop method (the drop sits suspended on a pedestal above the reservoir solution) or sandwich drop method, though rarely used (drops is sandwiched between two cover slits) [43].

Proteins and other macromolecules from living systems are sensitive to their environment, and only tolerate narrow ranges of temperature and pH, and must therefore be crystallized in an aqueous solution they can tolerate. The crystals are fragile and sensitive to disintegration, they break easily and take extensive damage from prolonged exposure to radiation. The level of detail in the diffraction pattern directly correlates with the crystals degree of internal order, and in turn the level of detail in atomic position. The position and orientation of the molecules in the crystal may differ between unit cells, causing limited resolution of the diffraction patterns. The degree of internal order is mostly limited by the high amount of solvent in the crystals that fill the liquid channels and cavities in the protein. Protein crystals are composed of 25-90% solvent, depending on the molecule, but usually around 50%, where the remainder are macromolecules [46]. Because of the large amount of solvent in the crystals, the individual macromolecules are surrounded by water, causing the structure to remain virtually unchanged from their structure in solution. This also goes for their ligand binding, enzymatic and spectroscopic characteristics. Consequently, chemical compounds such as ions, ligands, inhibitors, and substrates amongst others can be freely diffused in and out of the crystals. It is therefore possible to experiment with soaking the crystals in solutions of the previously mentioned compounds [41].

2 Materials and methods

2.1 Protein evolution, expression, and purification

OXA-48:F72L was identified as a single variant conferring increased ceftazidime resistance and strong fitness benefits. The OXA-48 variant OXA 48:A33V/K51E/F72L/S212A/T213A (OXA-48:Q5) was selected from five rounds of directed evolution conferring increased resistance to ceftazidime, a β-lactam with high clinical relevance. The protein samples used for all experiments were previously purified by Christopher Fröhlich as described in [8].

In brief, cultures of *Escherichia coli (E.coli)* BL21 AI carrying either pDEST17-bla$_{OXA-48}$ or the corresponding OXA-variants were grown to OD$_{600}$ of 0.4 in terrific broth with 100 mg/L ampicillin at 37°C and expression was induced by adding L-arabinose at a final concentration of 0.2% (Sigma-Aldrich). Expression was carried out for 16 h at 15°C and cells were harvested through centrifugation at 4°C for 30 minutes. All enzymes were produced without their signal peptide, but a 6x His tag followed by a TEV cleaves site were at the N-terminus. Cells were lysed by sonication and lysate was cleared by centrifugation (50000g, 4°C, 30 min), then loaded on a 1 mL HisTrap crude column equilibrated with 25 mM Sodium HEPES pH 6.5 and 50 mM K$_2$SO$_4$. Proteins were eluted with a linear gradient over 30 column volumes using a buffer supplemented with 500 mM imidazole, 25 mM HEPS pH 6.5, and 50 mM K$_2$SO$_4$. The His tag on the corresponding enzymes was cleaved by overnight dialysis with an in-house produced His-tagged TEV protease in a 1:10 ratio (OXA-48:TEV)against 25 mM HEPS pH 6.5, 25 mM K$_2$SO$_4$, 1 mM EDTA, and 2 mM 2-mercaptoethanol. The dialyzed sample was loaded a second time on HisTrap column, where the flow-through contained the corresponding, cleaved OXA-48 variants.

2.2 Steady-state enzyme kinetics

In order to determine k_{cat}/K_m a phosphate buffer saturated with carbonate was used (Table 2A). The carbonate was added to ensure carboxylation of K73 in the active site [47].

Table 2A: Solutions used in the enzyme kinetics assays.

	Contents with final concentrations
Buffer A	78 mM NaH_2PO_4 122 mM Na_2HPO_4
Buffer B	39 mM NaH_2PO_4 61 mM Na_2HPO_4 50 mM $NaHCO_3$

Prior to measuring the final enzyme kinetics, different concentrations of the protein samples were tested and optimized, to ensure good signal to noise ratio. Enzyme concentration was determined using a NanoDrop 2000 (Thermo Scientific) spectrophotometer at absorbance OD_{280}. 2 μL of buffer B (Table 2A) was used as the blank sample, and 2 μL of the protein sample was used for the measurement. The online program ExPASy was used to determine the extinction coefficients [48]. The concentration was calculated with Equation 2A by the NanoDrop software using the absorption measured (OD), the extinction coefficient ($\Delta\varepsilon$) and the molecular weight (MW) given in Table 2B.

$$\text{Equation 2A} \qquad [Protein] = \frac{OD(A280) \times Mw}{\Delta\varepsilon}$$

Table 2B: Extinction coefficients and molecular weight of OXA-48 wt and the two mutants.

Protein	Extinction coefficient, $\Delta\varepsilon$ ($M^{-1}cm^{-1}$)	Molecular weight (Da)
OXA-48:wt	63940	28204
OXA-48:F72L	63940	28170
OXA-48:Q5	63940	28108

2.2.1 Optimization of enzyme concentration

In order to produce a reliable signal from the enzyme kinetic measurements of OXA-48 and the mutants, different protein concentrations were probed for the individual proteins. Initially the measurements of OXA-48:wt and OXA-48:F72L were performed using concentrations reported by Fröhlich *et al* [8]. The first measurements revealed the need for optimization of enzyme concentration for the mutants OXA-48:F72L and OXA-48:Q5. The enzyme was diluted in buffer B with a starting concentration of 500 nM for which a 1:2-fold serial dilution was prepared in a 96-well UV plate, in addition to a negative control with only buffer B. The substrate piperacillin or ceftazidime with a final concentration of 500 μM was added to each well. The measurements were done in a SpectraMax M4 (Molecular Devices) UV spectrophotometer running the program SoftMax Pro 7.1 software (Molecular Devices). Each run was measured in 12 second intervals for 45 minutes at 25°C at the corresponding wavelength given in Table 2C. The measurements were done in triplicates, and the data was analyzed in the program Prism 9 (GraphPad Software).

Table 2C: The extinction coefficients and wavelengths for the substrates piperacillin and ceftazidime used for performing the enzyme kinetics.

β-lactam class	Substrate	Extinction coefficient ($\Delta\varepsilon$) ($M^{-1}cm^{-1}$)	Wavelength (nm)
Penicillin	Piperacillin	-820	235
Cephalosporin	Ceftazidime	-9000	260

2.2.2 Michaelis-Menten enzyme kinetics experiments in steady-state

Based on the optimized enzyme concentrations, Michaelis-Menten enzyme kinetics were performed to determine the kinetic parameters for OXA-48:wt and the mutants OXA-48:F72L and OXA-48:Q5, for the hydrolyzation reactions of piperacillin and ceftazidime. Enzyme kinetics with the substrate piperacillin were measured at pH 5.2, 7.2 and 9.2 to determine the pH dependency of the hydrolysis. For the substrate ceftazidime, kinetics was only measured at pH 7.2.

The antibiotics piperacillin and ceftazidime were dissolved in Milli-Q water to a 10 mM stock solution and diluted in buffer B (Table 2A) yielding in final concentrations of 9.375-800 μM, within the linear range of the spectrophotometer. The proteins OXA-48:wt, OXA-48:F72L and OXA-48:Q5 were diluted in buffer B to concentrations of 1 nM, 150 nM and 20 nM for piperacillin and 500 nM, 1000 nM and 10 nM for ceftazidime respectively (Table 2D). The measurements were performed in 96-well UV plates in a SpectraMax M4 (Molecular Devices) UV spectrophotometer running the program SoftMax Pro 7.1 software (Molecular Devices). All dilution series were measured as two parallel runs. The assays were run at 25°C for 45 minutes, with reading intervals of 12 seconds. The program GraphPad Prism 9 was used to analyze the data.

Table 2D: The final concentration of enzyme used for the kinetic measurements with piperacillin and ceftazidime.

Enzyme	Piperacillin (nM)	Ceftazidime (nM)
OXA-48	1	500
OXA-48:F72L	150	1000[a]
OXA-48:Q5	20	10[b]

[a] Value from Fröhlich *et al* [8].

[b] Fröhlich *et al.* (unpublished data).

2.3 Differential scanning fluorometry (DSF)

DSF was performed in the presence of the chemical denaturant urea to measure the effect of amino acid substitutions within OXA-48:F72L and OXA-48:Q5 on folding and thermostability in compared to OXA-48:wt. Using an MJ minicycler (Bio-Rad), melting curves were recorded between 20 and 80°C with 0.2°C increments per 5 seconds, or a heating rate of 2.4°C per minute, in the absence and presence of 2, 4, 6 and 8 M urea. The thermostability was determined in a solution of buffer A (Table 2A) at pH 7.2 and 4x SYPRO orange (Sigma-Aldrich) with 34 nM for OXA-48:wt, 42 nM for OXA-48:F72L or 62 nM for OXA-48:Q5. All measurements were performed in triplicates. The melting temperature (T_m) was determined by the first derivative of the melting curve using CFX Manager 3.1 (Bio-Rad). In addition, manual integration was applied for some measurements where the initial fluorescence was too high for automatic determination.

2.4 Urea kinetics

Kinetics were performed similarly to described in section 2.2. However, instead of testing pH dependency, different concentrations of urea were tested to see the effect of the amino acid substitutions on catalytic efficiency in the presence of urea. The kinetics were performed using 1, 2, 4, 6 and 8 M urea. All experiments were performed at pH 7.2 with the substrate piperacillin at a final concentration of 600 μM, diluted in buffer B (Table 2A). The assays were measured the same way as described in section 2.2 at 25°C, with the enzyme concentrations given in Table 2D. All measurements were performed in triplicates. For these kinetic experiments, full Michaelis-Menten kinetics were not performed as the activity was only measured at one substrate concentration.

2.5 Crystallization

Structural studies and analysis of changes within the enzymatic structure of the OXA-48:wt and the mutants OXA-48:F72L and OXA-48:Q5 were done using X-ray crystallography. Crystal structures of the variants in complex with different β-lactam substrates is desired to gain insight in the substrates binding to the enzyme. In order to study substrate binding, grown crystals were soaked in β-lactam containing solutions. Established crystallization conditions were utilized, in addition to finding new conditions for the variants. The following sub-chapters describe the crystallization conditions and optimization process for the three proteins.

2.5.1 Crystallization of OXA-48:wt

Crystallization conditions for several variants of OXA-48 including the wt were previously found by master student Birgit Nesheim and consisted of 0.1M BIS-Tris propane pH 9.0 and 9.5, 14-18% PEG MME 5000 [49]. Based on these conditions a 24-well plate was set up manually with the hanging drop method using a gradient by column of PEG MME 5000 and pH gradient by row, with two 2 μL drops with 1:1 and 1:2 ratio of protein to reservoir solution on each cover slide [41]. The plate was stored at 4°C. As this produced promising results with many small crystals, several more 24-well plates were set up using Formulator Liquid dispenser (Formulatrix), with three drops on each slide, with 1:2, 1:3 and 1:4 ratio. Final conditions for grown crystals can be seen in Table 2E.

2.5.2 Crystallization of OXA-48:Q5

For OXA-48:Q5 new crystallization conditions were desired. Four commercial 96-well plate sitting-drop crystallization screens; PGA, Pact Premier, Structure I+II and SG1 (Molecular Dimensions) were set up using the robot NT8 – Drop Setter (Formulatrix) [41]. Crystallization conditions from well C7 from the SG1 screen were selected for further optimization, containing 0.1M Sodium HEPES pH 7.5 and 25% w/v PEG MME 3350. The crystals grown under these conditions are displayed in Figure 3G. Based on these results from the initial screening a 24-well plate was set up using Formulator Liquid dispenser (Formulatrix), with a gradient of pHs of pHs from 6-8.5 with 0.1 M Sodium HEPES and 20-35% PEG MME 3350. The plate was set up with three hanging drops in each well, with ratios of 1:1, 1:2 and 2:1 of protein to reservoir solution. Conditions used for the diffracting OXA-48:Q5 crystal is shown in Table 2E.

2.5.3 Crystallization of OXA-48:F72L

Two 24-well plates were set up, one with the crystallization conditions used for OXA-48:wt, and one with the same conditions used for OXA-48:Q5. The variant OXA-48:F72L was crystallized using the same conditions as OXA-48:Q5, with final crystallization conditions for the crystal grown in Table 2E.

Table 2E: Crystallization conditions for crystals obtained of OXA-48:wt and variants OXA-48:F72L and OXA-48:Q5.

Protein	OXA-48:wt	OXA-48:F72L	OXA-48:Q5
Method	Vapor diffusion		
Plate-type	Hampton Research VDX 24-well plate with sealant		
Protein concentration (mg/mL)	7.95	12.31	9.79
Composition of reservoir solution	0.1 M BIS-Tris propane pH 8.0-9.3, 18-21% PEG MME 5000	0.1 M Sodium HEPES pH 7.5, 23% PEG MME 3350	0.1 M Sodium HEPES pH 7.5, 23% PEG MME 3350
Reservoir volume (μL)	500	500	500
Total drop volume (μL)	2	2	2
Ratio of reservoir solution to protein	1:1 and 1:2	1:4	1:3

2.5.4 Crystal soaking, freezing, data collection and refinement

The crystals were soaked in a cryoprotection solution containing reservoir solution and 20% ethylene glycol, and this solution was saturated with either piperacillin or ceftazidime prior to flash freezing in liquid nitrogen and exposure to X-rays at European Synchrotron Radiation Facility (ESRF). The goal was to capture the substrate in the active site to gain insight in binding of the substrate. The following soaking experiments were performed:

1) OXA-48:wt crystals were initially soaked in either piperacillin or ceftazidime for a couple minutes, but as this was unsuccessful, a new attempt was made with new crystals where some crystals were soaked for 10-15 minutes in piperacillin and some crystals were soaked overnight in ceftazidime at 4°C.

2) OXA-48:F72L was successfully crystallized, and data was collected, however due to time-constrains the data was not analyzed in this thesis.

3) OXA-48:Q5 crystals were soaked for 15 minutes in the cryoprotection solution with piperacillin

Structural data was collected, and the structure solved and refined by Christopher Fröhlich and Hanna-Kirsti S. Leiros using Phenix [50]. Analysis of the refined structures was performed in PyMOL and LigPlot+ [51, 52].

3 Results

3.1 Steady state enzyme kinetics

Within this study, one aim was to understand the catalytic relevance of the amino acid changes acquired during laboratory evolution. Enzyme kinetics were performed on OXA-48:wt and the mutants OXA-48:F72L and OXA-48:Q5 with the substrates piperacillin at pH 5.2, 7.2 and 9.2 and ceftazidime at pH 7.2 only, to study the effects of different amino acid changes and pH values on the enzymes activity.

3.1.1 Method optimization

The measured protein concentrations of the samples used for the enzyme kinetics are given in Table 3A.

Table 3A: Protein sample concentration of OXA-48 and the two mutants used in the kinetic studies.

Enzyme	Concentration (μM)
OXA-48:wt	281
OXA-48:F72L	347
OXA-48:Q5	515

To obtain a significant signal in the enzyme kinetics, optimization of enzyme concentrations was needed for the mutant OXA-48:F72L and OXA-48:Q5. For an overview of the final concentrations selected for each mutant see Table 2D. Examples of the results can be seen in Figure 3A which shows a comparison between an enzyme concentration of 7.8 nM, which produced a signal only 1.8 times higher than the background reaction, and 16 nM which produced a signal 2.6 times higher than the background reaction. Aiming for a signal that was around 3 times the background reaction, the mutant OXA-48:Q5 had to be increased to 20 nM, 20 times higher than the wt. The concentration of OXA-48:F72L had to be increased to a final concentration of 150 nM to obtain a significant signal, which is 150 times higher than concentration used for the wt.
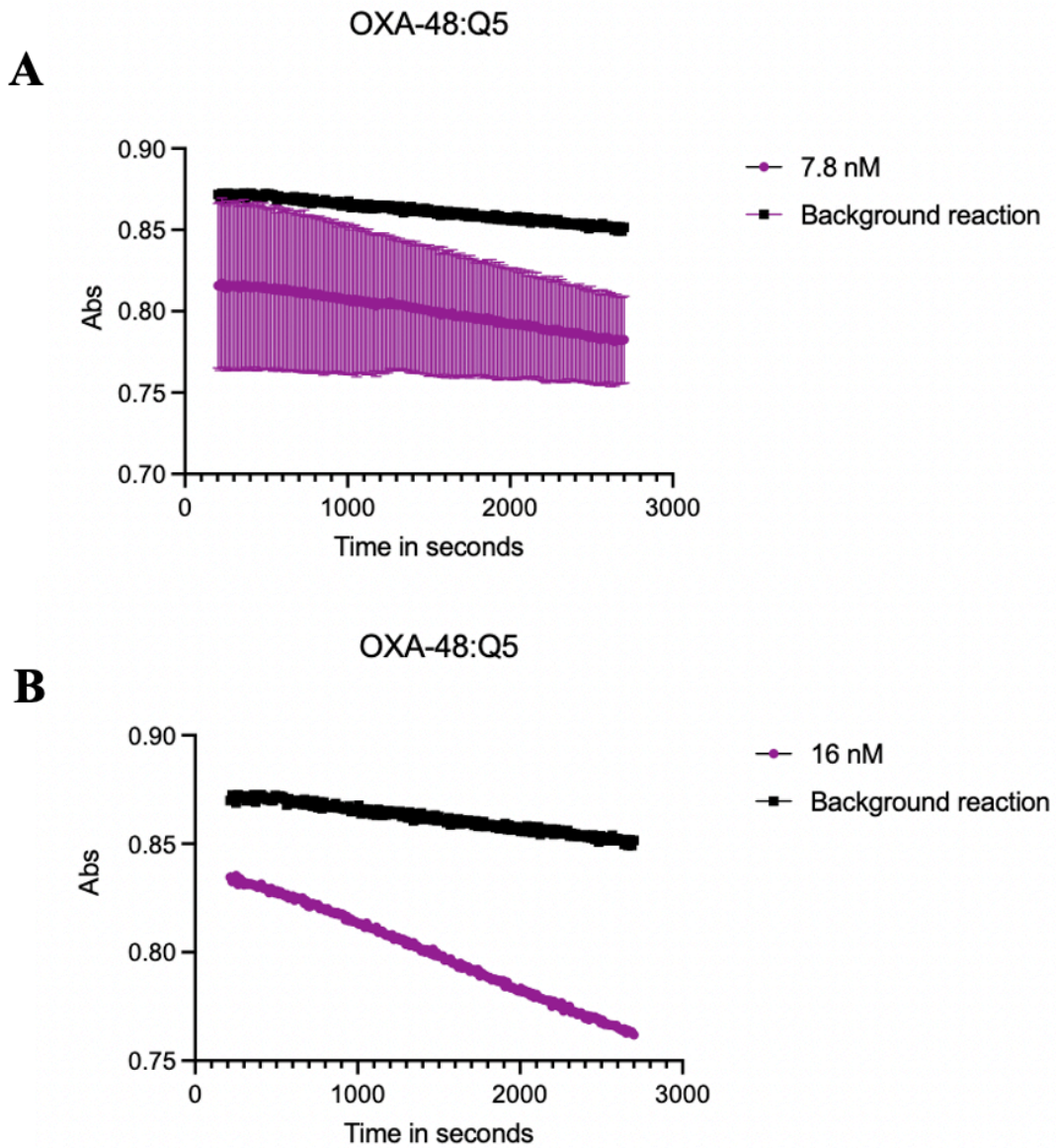
Figure 3A: Plot of absorbance over time in seconds for two enzyme concentrations used in optimizing the enzyme concentration of OXA-48:Q5. A) shows the slope at 7.8 nM (purple) and the background reaction (black) and B) shows the slope at 16 nM (purple) and the background reaction (black).

3.1.2 Effect of the pH on catalysis

Enzyme kinetics were performed for the three proteins at pH 5.2, 7.2 and 9.2 with the substrate piperacillin and are shown in Figure 3B. The kinetic values K_m, k_{cat} and K_m/k_{cat} are shown in Table 3B. For the substrate ceftazidime only results for OXA-48:wt at pH 7.2 was successfully obtained. Results from previous studies are included in the table for comparison. A comparison of the mutants at pH 7.2 is shown in Figure 3C. The individual Michaelis-Menten curves are supplemented in Appendix A1-A3.

Firstly, while OXA-48:F72L and OXA-48:Q5 improved the catalytic efficiency against ceftazidime by 35-fold and 32-fold respectively, the catalytic efficiency against the substrate piperacillin displayed a 117-fold and 12-fold reduction compared to the wt at pH 7.2. This suggests that OXA-48:Q5 regains the catalytic efficiency against piperacillin more so than OXA-48:F72L. With the substrate piperacillin OXA-48:F72L showed no substantial change in K_M, but a 120-fold decrease in k_{cat} compared to the wt. For OXA-48:Q5 K_M decreased by a 3-fold, and k_{cat} decreased by a 40-fold. With the substrate ceftazidime OXA-48:Q5 showed a 64-fold increase in k_{cat} and a 200-fold increase in K_m compared to the wt. This suggests that both the catalytic turnover and the binding affinity has increased due to amino acid changes in OXA-48:Q5 compared to the wt. For OXA-48:F72L k_{cat} and K_m values were not determined.

Next, the effect of lower and higher pH values on catalysis was investigated. All mutants showed decreased activity towards piperacillin at pH 5.2 compared to their activity at pH 7.2 and 9.2, around a 10-fold reduction, which indicates that the activity of OXA-48 is pH dependent. OXA-48:wt showed no substantial change in K_m at the different pHs but shows a 3.6-fold decrease in k_{cat} at pH 5.2. Both mutant OXA-48:F72L and OXA-48:Q5 shows a decrease in both K_m and k_{cat} values at pH 5.2 compared to their values at pH 7.2 and 9.2. At pH 9.2 the catalytic efficiency had a decrease of a 1.2-fold change for OXA-48:wt, a 1.2-fold for OXA-48:F72L and a 1.4-fold for OXA-48:Q5.
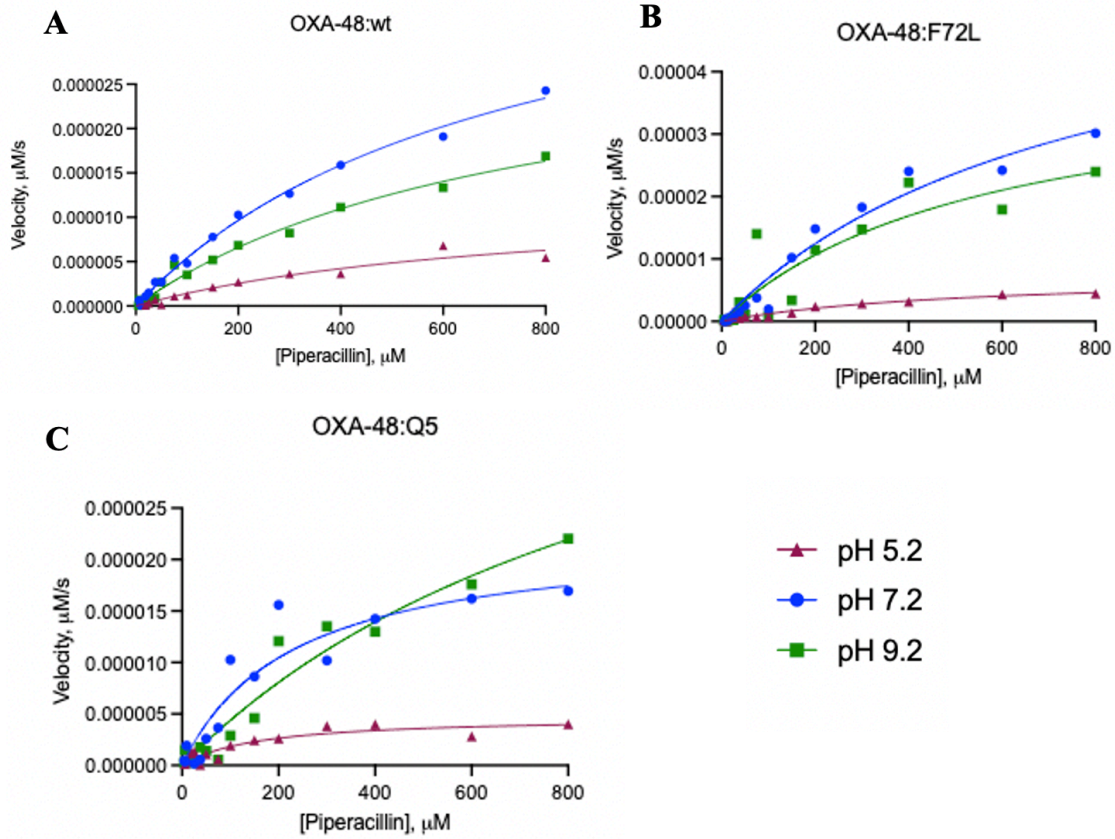
Figure 3B: Michaelis-Menten curves for wild type OXA-48 and the two mutants with the substrate piperacillin at pH 5.2 (red), 7.2 (blue) and 9.2 (green). A) OXA-48:wt using 1 nM, B) OXA-48:F72L using 150 nM, C) OXA-48:Q5 using 20 nM.
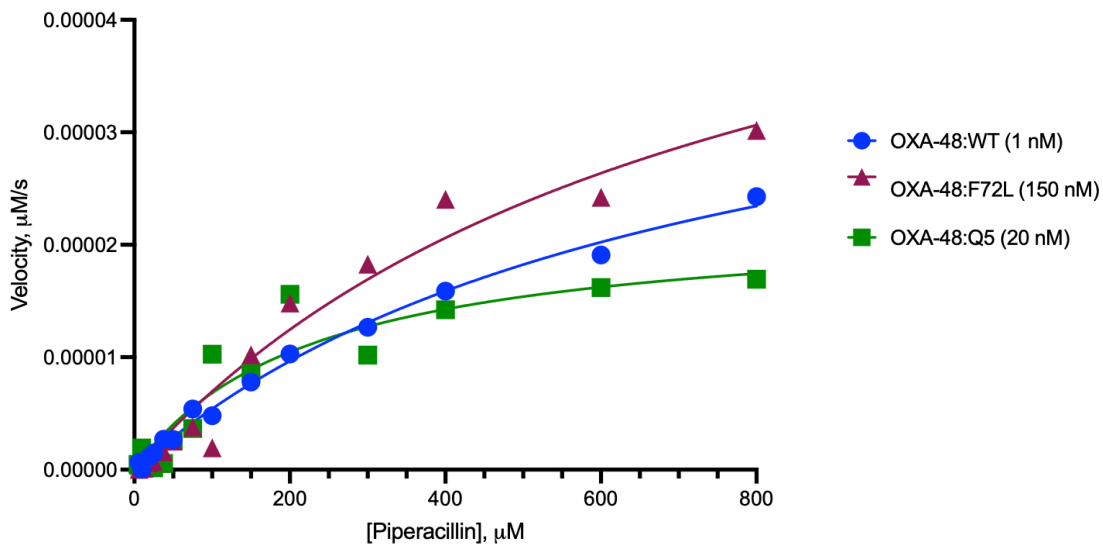
Figure 3C: OXA-48:wt and the two mutants at pH 7.2 for the substrate piperacillin, concentrations for the three variants used are showed in the figure.

Table 3B: Kinetic values K_m, k_{cat} and catalytic efficiency k_{cat}/K_m for OXA-48:wt and the mutants OXA-48:F72L and OXA-48:Q5 with the substrates piperacillin and ceftazidime [a].

Substrate	pH	OXA-48:wt			OXA-48:F72L			OXA-48:Q5		
		K_m (µM)	k_{cat} (s⁻¹)	k_{cat}/K_m (M⁻¹s⁻¹)	K_m (µM)	k_{cat} (s⁻¹)	k_{cat}/K_m (M⁻¹s⁻¹)	K_m (µM)	k_{cat} (s⁻¹)	k_{cat}/K_m (M⁻¹s⁻¹)
Piperacillin	5.2	764.8 ± 329	394.1 ± 12	$5.15 \cdot 10^5$	535.7 ± 196	1.6 ± 0.6	$3.07 \cdot 10^3$	159.6 ± 62	7.6 ± 1	$4.77 \cdot 10^4$
	7.2	726 ± 96.8	1435.2 ± 72	$1.98 \cdot 10^6$	758.7 ± 246	12.8 ± 2	$1.68 \cdot 10^4$	229.2 ± 86	36.0 ± 6	$1.57 \cdot 10^5$
	9.2	771.4 ± 166	1029.5 ± 133	$1.33 \cdot 10^6$	569.3 ± 366	7.5 ± 2.7	$1.32 \cdot 10^4$	1078 ± 521	82.7 ± 27	$7.67 \cdot 10^4$
Ceftazidime	7.2	325.6 ± 84	0.10 ± 0.01	$3.12 \cdot 10^2$	N/D	N/D	$1.1 \cdot 10^{4}$ [b]	720 ± 620 [c]	6.4 ± 3.8 [c]	$1.0 ± 0.2 \cdot 10^{4}$ [c]

N/D: not determined

[a] Errors are reported as standard error of the mean.

[b] Fröhlich *et al.* [8].

[c] Fröhlich *et al.* (unpublished data).

3.2 Differential scanning fluorimetry

Differential scanning fluorometry was performed to assess the thermostability of the variants compared to the wt, to investigate whether or not evolving OXA-48 towards increased ceftazidime resistance came with a trade-off in terms of its thermostability, as functional mutations of other β-lactamases have shown to decrease the thermostability of the enzymes [30, 53]. Additionally, the chemical denaturant urea was added to hopefully gain insight into the changes in intermolecular forces and how the mutations affect the proteins thermostability in presence of a denaturant.

One of the main ways to assess protein stability and the effects of mutations on the proteins stability and its unfolding is to use the agent urea to chemically denature the protein [54]. The molecular basis for ureas ability to denature proteins is unknown, however there are two mechanisms proposed to explain the denaturing of the proteins: indirectly and directly. Indirectly urea alters the solvent environment by disrupting the water structure which diminishes the hydrophobic effect, making the proteins hydrophobic core residues less compact and more readily solvated. The direct mechanism proposes that urea actively participates in unfolding process by competing with native electrostatic interactions or forms preferential van der Waals interactions with protein residues. The direct mechanism also proposes that urea binds to the denatured state, thereby stabilizing it [54-56]. It is suggested that both mechanisms can play a role in ureas ability to denature proteins.

Differential scanning fluorometry was performed on all three enzymes, both in the absence and presence of 2, 4, 6 and 8 M urea. The resulting melting temperature (T_m) slopes can be seen in Figure 3D, with the individual T_m values in Table 3C. Examples of the resulting melting curves can be seen in Figure A4 in the Appendix for 0 and 4 M urea. With no urea present the thermostability of variant OXA-48:F72L decreased by 6.5°C when compared to the wt, and the variant OXA-48:Q5 decreased by 6.4°C compared to the wt. The difference between the mutants increases with larger concentrations of urea, except for 6 M, however, for the wt the melting temperature was as mentioned determined manually, which lowers the accuracy and validity of the results. The confidence intervals of the resulting slopes do not overlap, which suggests that the differences in thermostability are substantial. OXA-48:Q5 generally exhibited

a greater decrease in melting temperature than OXA-48:F72L, which suggests that this enzyme is less thermostable than OXA-48:F72L and the wt.
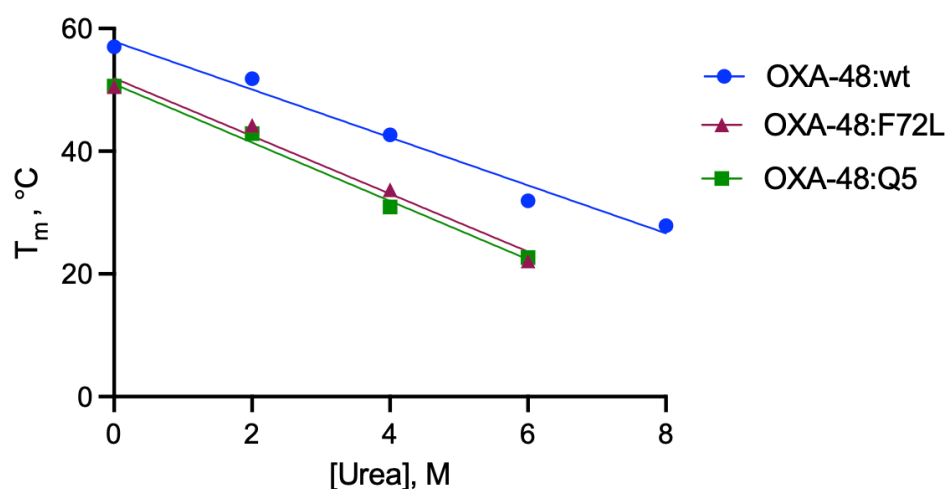
Figure 3D: Shows the T_m values in °C plotted against the concentration of urea in M. The slopes of the graphs shown as confidence intervals are: wt: -3.6 to -4.2°C/M, F72L: -4.2 to -5.2°C/M, Q5: -4.4 to -5.1°C/M. The graph includes the manually determined values as specified in Table 3C.

Table 3C: Shows the melting temperatures (T_m) for the three enzymes OXA-48:wt, OXA-48:F72L and OXA-48:Q5 with standard error of the mean given, and the difference to OXA-48:wt for the two mutants.

|	Melting temperature (T_m) in °C			ΔT_m in °C	ΔT_m in °C
Concentration of urea	OXA-48:wt	OXA-48:F72L	OXA-48:Q5	OXA-48:F72L	OXA-48:Q5
0 M	57.0 ± 0.1	50.5 ± 0.1	50.6 ± 0.1	-6.5	-6.4
2 M	51.8 ± 0.28	44.2 ± 0.1	42.9 ± 0.1	-7.6	-8.9
4 M	42.7 ± 0.1	33.7 ± 0.25	30.9 ± 0.5	-9	-11.8
6 M	31.9 ± 0.47^a	N/D	N/D	N/D	N/D
8 M	27.9 ± 0.57^a	N/D	N/D	N/D	N/D

N/D: not determined.

[a] Determined manually as described in section 2.1.

3.3 Urea kinetics

Mutations that affect the function of the enzyme have also been shown to alter other characteristics of the protein such as folding and binding [57]. Determining the unfolding effect of urea on proteins activity may therefore shed light on differences in intramolecular interactions. Thus, in case of OXA-48, steady-state enzyme kinetics were performed in the presence and absence of urea to study its effect on the catalytic efficiency.

Steady-state kinetics without urea were recorded and the values obtained for each mutant were used for normalization and represented 100%. At 1 M urea OXA-48:wt retained 90% of its activity, whereas the activity of OXA-48:F72L and OXA-48:Q5 decreased to 60% and 75%, respectively. At 2 M OXA-48:wt had an activity of only 31%, whereas OXA-48:F72L had an activity of 66% and OXA-48:Q5 showed 53% activity, whereas at 4 M the variants exhibited an activity of 30, 37 and 3% respectively. At 6 M OXA-48:wt only showed an activity of 13%, and the two mutants both displayed a 5% activity. All three variants were considered inactive at 8 M as no activity was measurable above the background signal. It should be noted that OXA-48:F72L has a much higher standard error of the mean than OXA-48:Q5 and only one reliable measurement was obtained for OXA-48:wt, so these results should be seen as preliminary. Taken together, the activity of OXA-48:wt is retained well between 0 and 1 M but reduce drastically in the presence of 1 to 2 M urea, and at 4 M urea the activity for all three variants is below 50%. OXA-48:F72L showed the greatest urea dependency of the three variants, as close to 0% activity was exhibited at 4 M urea.
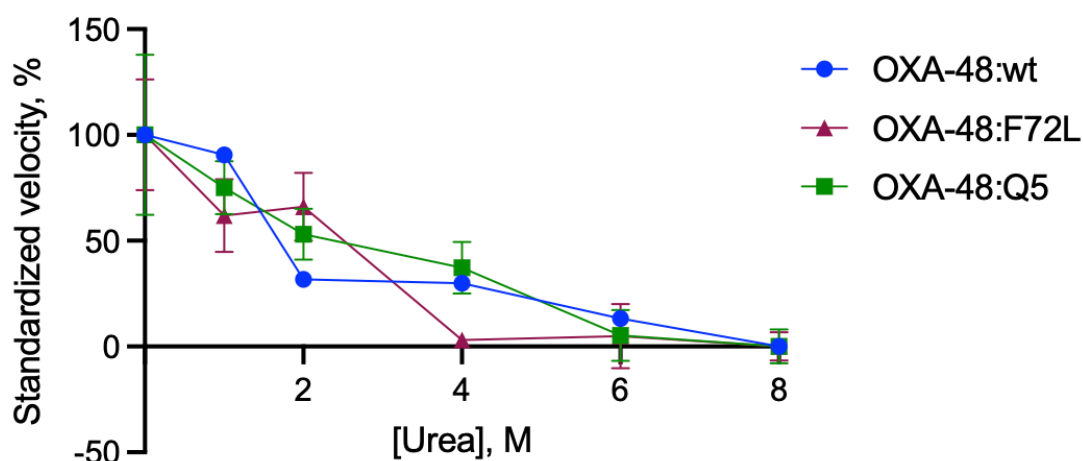

Figure 3E: Shows the relative activity in percentage for the enzymes with 0, 1, 2, 4, 6 and 8 M urea present. For OXA-48:wt only one reliable measurement was obtained. For the two mutants triplicate measurements were obtained and standard errors from the mean are shown in the graph.

3.4 Protein crystallization, X-ray data collection and modelling of the three OXA-48 mutants

3.4.1 Crystallization of the mutants

The main goal of the crystallization trials was to obtain structures of the mutants, and structures of the three proteins in complex with the substrate, to gain insight into the binding and structure of the protein when in complex with the substrate. To obtain crystals for structure determination crystallization trials were set up for the mutants OXA-48:wt, OXA-48:F72L and OXA-48:Q5.

For the OXA-48:wt, conditions were already available from previous studies, so plates were set up using these conditions, which included 0.1 M BIS-Tris propane at pH 8.0-9.3 and 18-21% PEG MME 5000 [49]. This resulted in several good quality crystals (Figure 3F), which were uniform and a suitable size for soaking. Crystallization conditions used for all mutants are displayed in Table 2E. Here, the goal was to study substrate binding and to capture the substrate piperacillin and ceftazidime in the active site of the protein. To do so, crystals were soaked in a cryoprotectant solution of reservoir solution, 20% ethylene glycol and saturated with either substrate. For the OXA-48:wt crystals were sent for X-ray data collection at two separate occasions, for the first attempt the crystals were soaked for a short time (1-2 minutes), and for the second attempt some of the crystals were soaked for 10-15 minutes for piperacillin, and some of the crystals were soaked overnight at 4°C for ceftazidime. For none of the OXA-48:wt crystals sufficient enough electron density was found and therefore no refined substrate complex could be obtained.
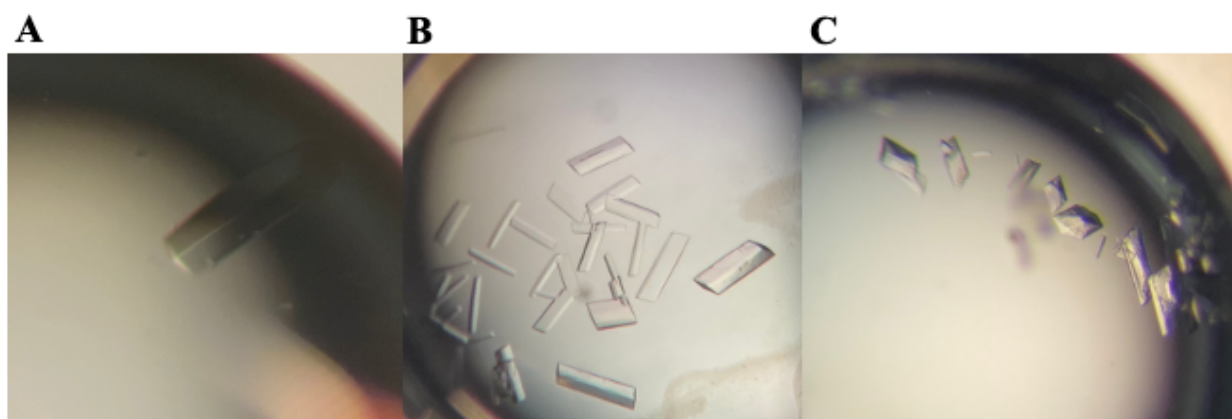
Figure 3F: Shows A) the OXA-48:F72L crystal, B and C) some of the OXA-48:wt crystals used from two different wells.

For the OXA-48:Q5 mutant, crystallization conditions were not known, and commercial screens were used to screen for suitable crystallization conditions. Using the SG1 screen (Molecular Dimensions), crystal formation under 0.1 M Sodium HEPES pH 7.5 and 25% w/v PEG MME 3350 could be observed (Figure 3G). To improve crystallization conditions, a screen was set up manually using a HEPES pH gradient from 6.0 to 8.5 and a PEG 3350 gradient from 20 to 35% w/v. This refinement clearly improved the crystal form and shape (Figure 3G) and resulted in the final conditions used for structure determination (Table 2E). Figure 3G shows the progression of the crystals grown of OXA-48:Q5 from the initial screen to the final crystals used for data collection. In total, six crystals of the OXA-48:Q5 mutant were soaked in a saturated piperacillin cryoprotectant solution of reservoir solution containing 20% ethylene glycol for 10-15 minutes and were sent for X-ray data collection. Piperacillin was captured successfully in the OXA-48:Q5 mutant at a resolution of 1.5 Å. The crystal structure was solved and refined by Christopher Fröhlich and Hanna-Kirsti S. Leiros. X-ray data collection and statistics for the structure can be seen in Appendix Table A1. A figure of the solved structure with an electron density map of the substrate can be seen in Figure 3H.

For OXA-48:F72L, two plates were set up for the crystallization where one had the same conditions as OXA-48:wt and the other the same conditions as for the OXA-48:Q5 mutant. One crystal was obtained from the plates, with the conditions 0.1 M Sodium HEPES pH 7.5 and 23% PEG MME 3350. The crystal of the mutants F72L was sent for X-ray data collection, and provided enough electron density to be refined, but due to time constraints the structure from this crystal will not be presented. A picture of the crystal used can be seen in Figure 3F.
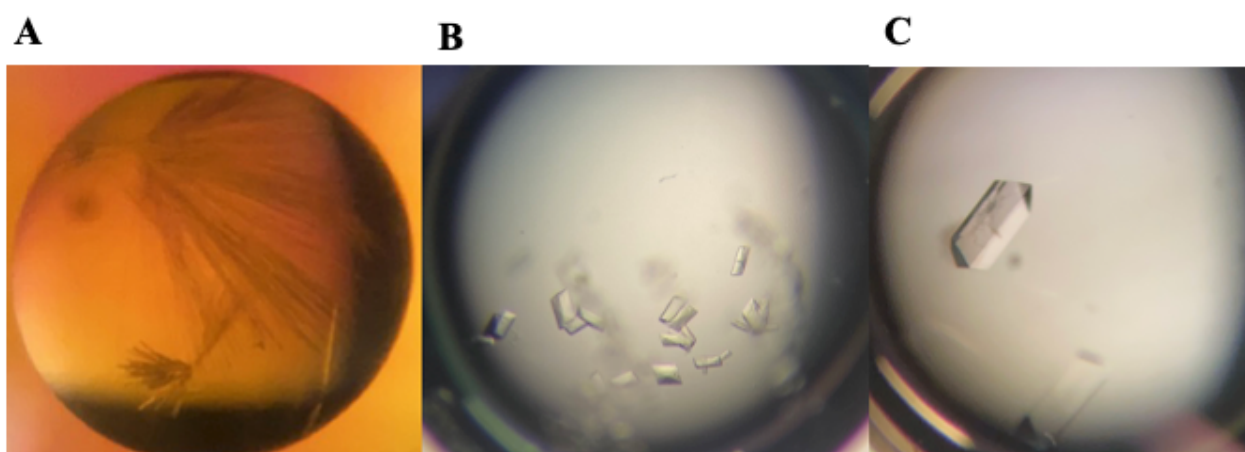

Figure 3G: Shows the progression of the crystals grown of mutant OXA-48: Q5 from A) the initial screening to B) the first plates from the manually set up pH and PEG MME gradient to C) one of the final crystals used for data collection.

3.4.2 Structural analysis of OXA-48:Q5 complexed with piperacillin

X-ray crystallography was performed on crystals of OXA-48:Q5 soaked in piperacillin to analyze the structure of the mutant, mainly to see if the structure can shed light on the functional trade-off observed, and study substrate binding.

The substrate piperacillin was successfully captured in the active site, covalently bound to OXA-48:Q5, and the crystal structure has two more piperacillins present in the molecule. An overview of the structure and the electron density maps for the piperacillin molecules can be seen in Figure 3H. In the refined structure analyzed residues 153-158 within the Ω-loop are not displayed due to lacking electron density.
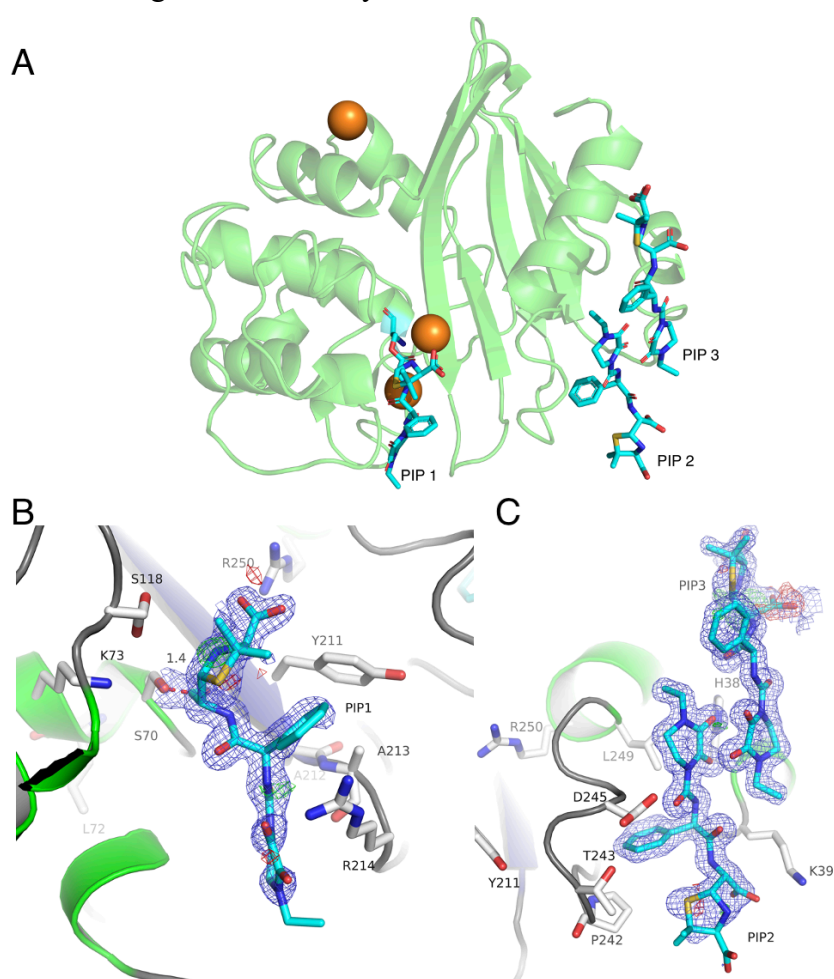
Figure 3H: Shows A) ribbon structure of OXA-48:Q5 (green) with three piperacillin molecules present (cyan). Chloride ions are shown in orange. Electron density maps of B) piperacillin in the active site of OXA-48:Q5 and C) two piperacillin molecules. The $2F_o$-F_c map is displayed at 1.3 σ (blue) and the F_o-F_c maps are displayed at +3.5 σ (green) and –3.5 σ (red). β-sheets are displayed in dark blue, α-helices in green and loops in grey. Piperacillin is displayed in cyan and neighboring residues in white, where atoms are color coded according to atom type (carbon: white/cyan, blue: nitrogen, red: oxygen and yellow: sulfur). Figure B and C were made by Hanna-Kirsti S. Leiros.

31

First, the effect of the five mutations on the structure of OXA-48 was studied. The structure shows all five mutations, which are shown in Figure 3I. The mutations do not affect the overall fold of the enzyme, and the key active site residues S70 and K73 are still in the same position. However, as seen in the figure below, the Ω-loop is in a different orientation and seems to be more flexible based on the electron density in this region, which is in line with previous studies [8].
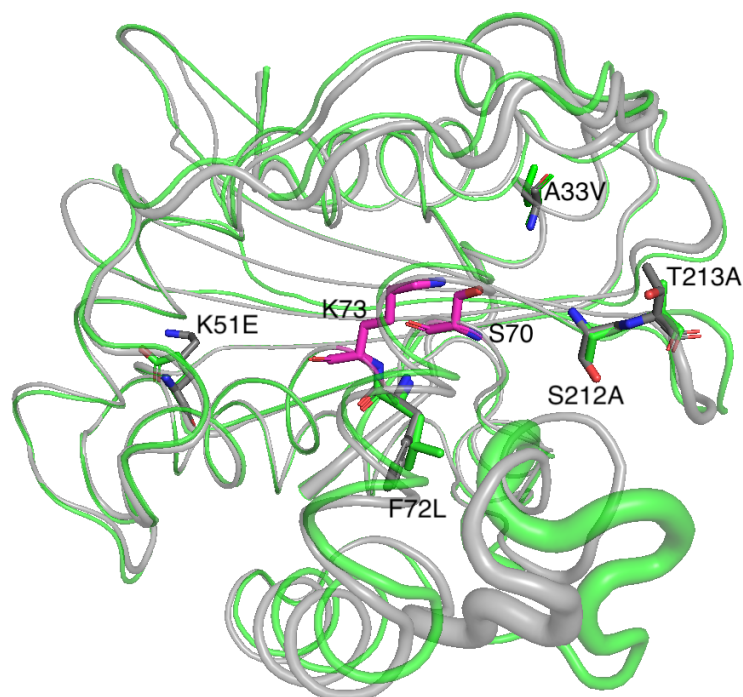
Figure 3I: Ribbon structure of OXA-48:Q5 in complex with piperacillin (green) overlayed with OXA-48:wt (grey) showing the mutations (PDB ID: 4S2P [58]). The key active site residues S70 and K73 (pink) are also included in the figure.

Second, substrate binding was studied. To do so, the structure was analyzed in PyMOL and LigPlot+ [51, 52]. The analysis showed that the enzyme has polar interactions with the piperacillin in the active site. The substrate is covalently bound to S70 and makes hydrogen bonds with residues Y211 and A213. PIP 1 also makes polar interactions with a chlorine ion which in turn makes polar interactions with T209 and R250. In addition, there are many hydrophobic interactions, which is shown in Figure 3J. Bonds and distances are summarized in Appendix Table A2.
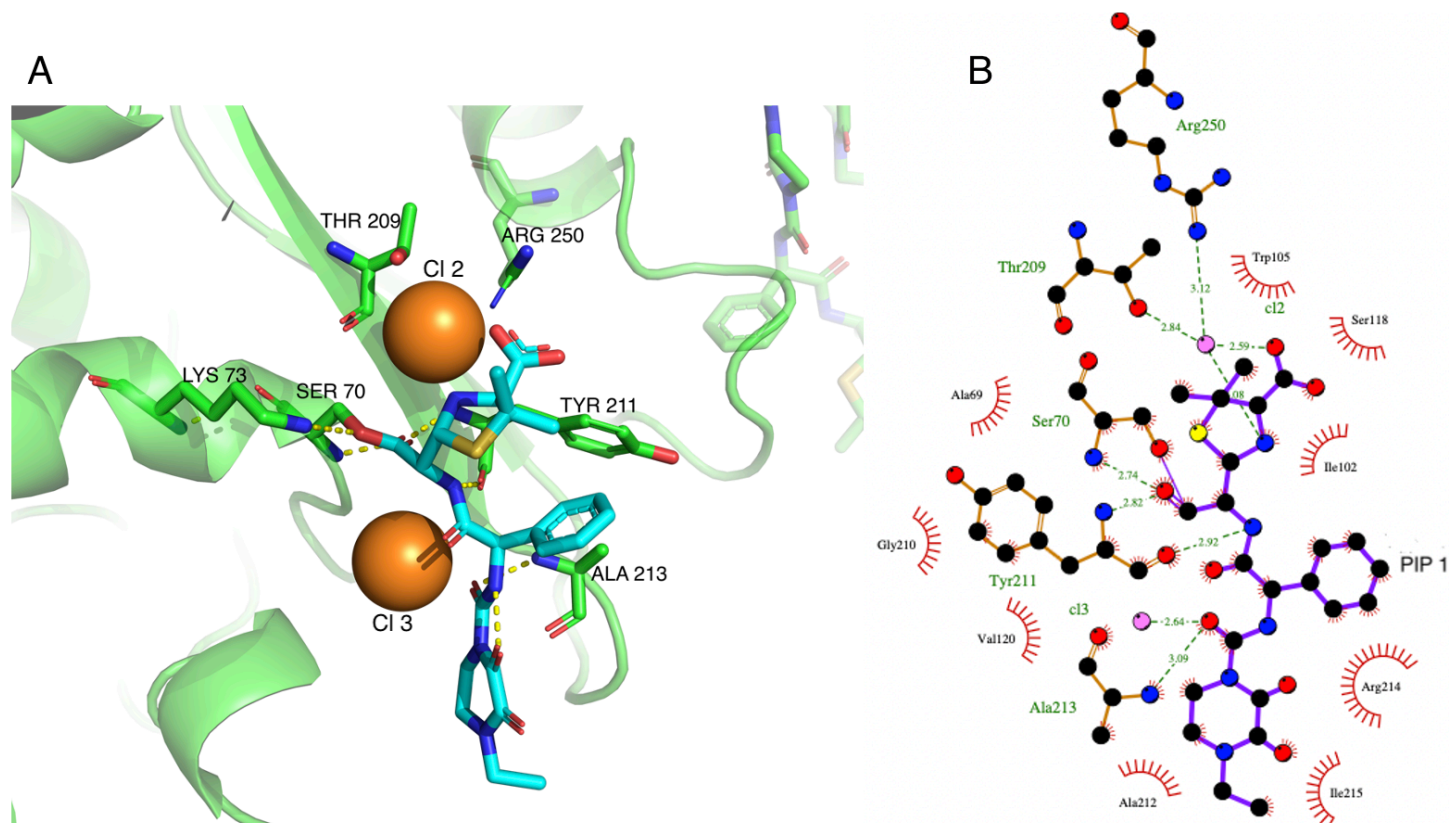
Figure 3J: Shows A) the active site of OXA-48:Q5 shown in green, and interactions shown with yellow dotted lines PIP1, which is shown in cyan. Chloride ions are shown in orange. B) interactions of PIP1 with the enzyme. Hydrogen bonds are shown as green dotted lines with the interatomic distances, and hydrophobic contacts are shown with red spline curves including the contacting residue in the enzyme. Chlorine ions are here shown in pink.

The interactions of the two piperacillins located on the surface of OXA-48:Q5 were also studied. PIP2 has polar interactions with H38 and K39 in addition to eight hydrophobic interactions, which are displayed in Figure 3K. Bonds and distances are summarized in Appendix Table A3. PIP3 has no polar interaction with the enzyme but does have hydrophobic interactions with the enzyme and PIP2.
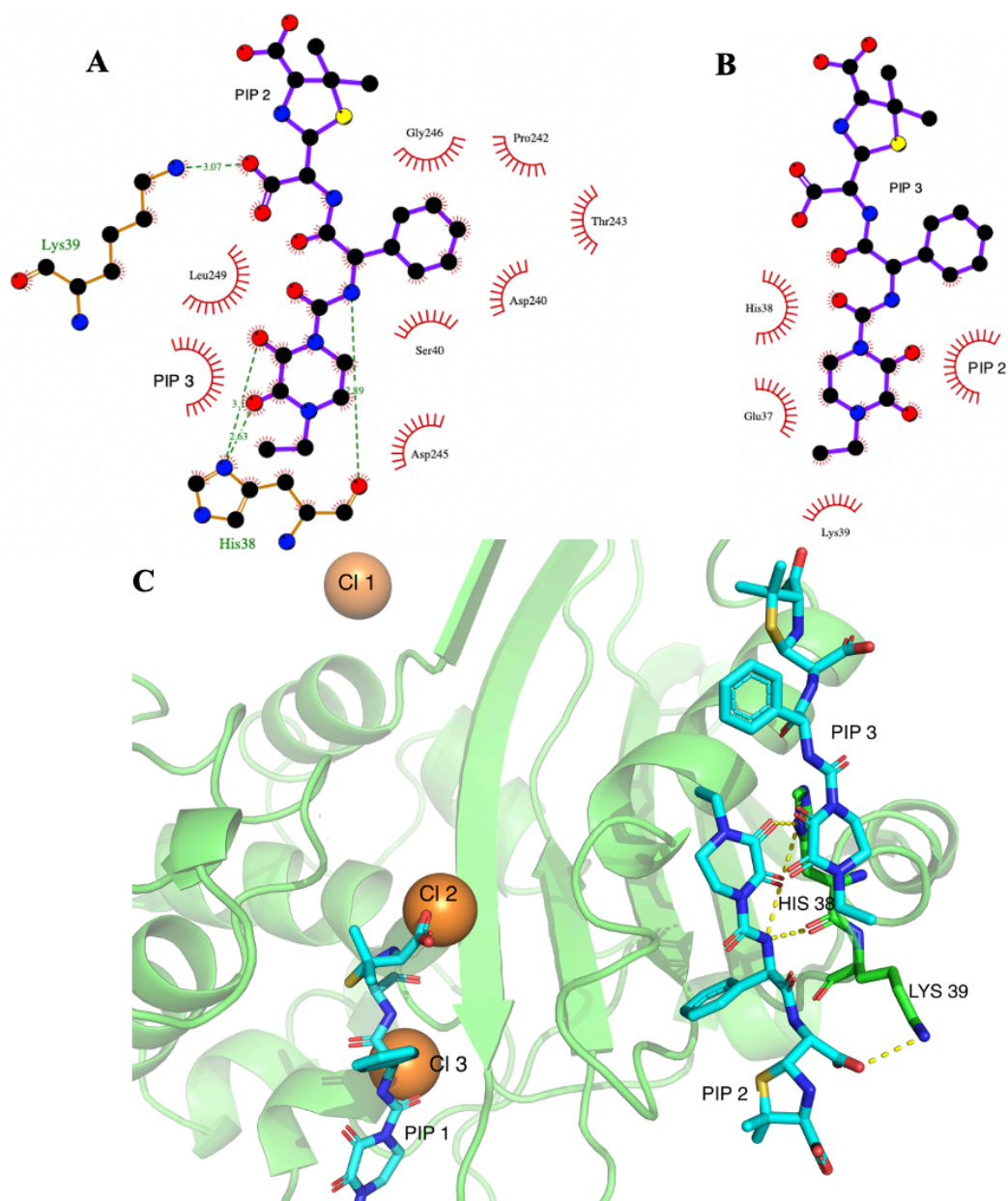
Figure 3K: Shows A) interactions between PIP2 and OXA-48:Q5 in complex with piperacillin. B) interactions between PIP3 and the enzyme. Hydrogen bonds and hydrophobic contacts are shown in the same way as in Figure 3J. C) PIP2 and PIP3 in OXA-48:Q5 shown the same way as in Figure 3J.

4 Discussion

4.1 pH-dependency within penicillinase activity

The effect of lowered and increased pH values on catalysis was investigated. OXA-48:wt, OXA-48:F72L and OXA-48:Q5 all displayed decreased activity at pH 5.2. K_M was not affected significantly in OXA-48:wt, but for OXA-48:F72L and OXA-48:Q5 there was a 1.4-fold decrease in K_M (Table 3B). However, the standard error is quite broad. There was a larger difference in the k_{cat} values, with OXA-48:wt having a 3.6-fold decrease, OXA-48:F72L having an 8-fold decrease, and OXA-48:Q5 having a 5-fold decrease. This suggests that the catalytic turnover is decreased more than the binding of the substrate. The catalytic efficiency k_{cat}/K_M for OXA-48:wt showed a 4-fold decrease in activity at pH 5.2 compared to pH 7.2. OXA-48:F72L showed a 5-fold decrease, and OXA-48:Q5 showed a 3-fold decrease.

At pH 9.2 the catalytic efficiency of all three variants did not display more than a 1.2-fold change for OXA-48:wt, 1.4-fold for OXA-48:F72L and 2-fold for OXA-48:Q5 compared to their activity at pH 7.2. There was a more substantial change in activity at pH 5.2 than at pH 9.2, in line with previous studies on other OXA enzymes that reported that lower pH can reduce the degree of carboxylation of K73, while full carboxylation is observed at higher pHs [47]. Previous studies have shown that carboxylation of K73 is necessary to carry out the enzyme mechanism shown in Figure 1D. Class D OXA-48 type β-lactamases have active sites which lower the pK_a of lysine due to hydrophobic residues of the active site, allowing carboxylation of K73 under physiological conditions. This is observed throughout Class D OXA-48 type β-lactamases and seem to be conserved throughout the three variants OXA-48:wt, OXA-48:F72L and OXA-48:Q5 [22, 47]. From the results represented here, the carboxylation dependency seems to be conserved for mutations, and a lowered pH seems to affect the catalytic turnover k_{cat} more than the Michaelis constant K_M. The pH can also affect enzymatic activity in other ways not discussed here in detail, like the charge of the enzyme, charge of the substrate, and the hydrolytic water (Figure 1D) among others.

4.2 Increase in catalytic efficiency against ceftazidime

OXA-48 has been described to only exhibit limited ability to catalyze the hydrolysis of the 3rd generation cephalosporin ceftazidime [7]. However, variants of OXA-48 conferring increased resistance against ceftazidime but decreased resistance against penicillins and carbapenems have emerged from natural evolution [10]. While these variants often show amino acid deletions, not much is known about the evolution of OXA-48 mediated ceftazidime resistance and related trade-offs through point mutations. In this work, steady-state enzyme kinetics was performed to gain understanding of the catalytic relevance of the amino acid substitutions acquired during evolution towards increased ceftazidime resistance in the previously evolved single mutation (OXA-48:F72L) and an optimized variant including five mutations (OXA-48:Q5).

To confirm that the mutations in fact do increase cephalosporinase activity withing OXA-48 steady-state enzyme kinetics were performed. OXA-48:wt, OXA-48:F72L and OXA-48:Q5 were tested with the cephalosporin ceftazidime to investigate the catalytic efficiency of the three variants. The kinetics revealed that the two evolved variants does indeed show increased catalytic activity compared to OXA-48:wt. OXA-48:F72L revealed a 35-fold increase in the catalytic efficiency k_{cat}/K_m, and OXA-48:Q5 a 32-fold increase relative to OXA-48:wt.

One hypothesis is that the mutations within OXA-48:Q5 increase flexibility within the Ω-loop (conserved within Class D β-lactamases, residue 140-168 [59]), which may aid in the binding of ceftazidime. Ceftazidime is a bulkier substrate, carrying a negatively charged oxyimino group, than piperacillin and the evolution towards ceftazidime resistance may change the structure of the Q5 mutated enzyme to adapt to these changes. The OXA-48:Q5 structure showed a conformational change of the Ω-loop (conserved withing Class D β-lactamases, residue 140-168 [59]) which can be seen in Figure 4A. Reshaping of the active site and changes in conformational dynamics are prevalent evolutionary mechanisms to enhance catalysis [60]. For example, in OXA-163, an OXA-48-like variant with increased ceftazidime hydrolysis, a crystal structure revealed that the active site of OXA-163 was expanded compared to OXA-48, allowing the bulky substrate ceftazidime to be accommodated [61]. Changes in conformational dynamics was for example observed in TEM-1, a class A β-lactamase, where a correlation was found between increased cefotaxime resistance and increased rigidity of its Ω-loop in designed variants [62].

However, the differences in the structure were elusive, and seeing how crystallography is based on static crystals, alternative methods such as NMR and molecular dynamic simulations would need to be used to understand the dynamical implications of the mutations.

4.3 Functional trade-offs

4.3.1 Methodical considerations

In order to understand how functional trade-offs within OXA-48 mutants arise, X-ray crystallography was performed.

Crystals of decent size and quality from OXA-48:wt were grown and soaked for a short time and for 10-15 minutes with the cryoprotectant solution saturated with either piperacillin or ceftazidime, yet no good crystal structure with bound substrate in the structure could be successfully obtained. To successfully obtain a complex for this enzyme co-crystallization with the substrate or crystallization with an inactive mutant, could possibly lead to a complex structure and this can be investigated in the future.

Crystallization trials of OXA-48:F72L were set up towards the end of the project time with existing conditions used for the other variants. Interestingly, only one crystal grew, and this single crystal had a good size and high quality, and an X-ray structure could be obtained. This shows why crystallization trials can be the rate-limiting step of the process of solving new crystal structures, as several crystals are usually required to successfully obtain a new structure, e.g., with soaking experiments of different substrates.

For OXA-48:Q5 new crystallization conditions were desired to obtain a new crystal structure in complex with piperacillin. The initial screening gave needle-like crystals of low quality and were not suitable to be used for X-ray crystallography (Figure 3G). The first plate that was sat up using the optimized conditions (Table 2E) gave some good crystals with the use of 1:1 and 1:2 ratios of reservoir solution to protein concentration, however many of them were grown together and smaller. With the use of the same reservoir solution, but with a 1:3 ratio (protein: reservoir solution) used, good size single crystals suitable for soaking were obtained. These crystals were larger and more uniform, leading to higher resolution in the final structure (Figure A5, Table A1) and good electron density maps of the enzyme in complex with piperacillin. The structure was solved to a resolution of 1.50 Å and showed piperacillin clearly in the active site, seen in Figure 3H.

4.3.2 Catalytic efficiency trade-offs towards piperacillin

For OXA-48, expansion of its substrate profile towards ceftazidime is seen to be accompanied with a trade-off towards carbapenems and penicillins, greatly reducing OXA-48 ability to catalyze the hydrolysis of penicillins and carbapenems [9, 10]. Therefore, steady-state enzyme kinetics were also tested with the penicillin piperacillin to explore the penicillinase activity.

Steady-state enzyme kinetic showed that the catalytic efficiency of both evolved variants had a decrease in activity compared to OXA-48:wt for the substrate piperacillin. OXA-48:F72L had a 117-fold decrease and OXA-48:Q5 had a 12-fold decrease in catalytic efficiency compared to OXA-48:wt towards piperacillin, respectively.

4.3.3 Structural view on the trade-offs

In order to understand whether the acquired mutations imposed structural changes in OXA-48:Q5 that are responsible for the functional trade-off against other β-lactams, the obtained structure of OXA-48:Q5 in complex with piperacillin was studied.

An overview of the structure showed that the enzymes overall fold remained unchanged, and the structure elements were highly conserved, except the Ω-loop, which was in a different orientation and seemed to be more flexible based on the electron density. Three chlorine ions were found in the active site of OXA-48:Q5, two in the active site and one at the surface as shown in Figure 3H and Figure 3J as orange spheres. For two of the ions (Cl2/Cl3; Figure 3J) this could indicate excess space in the active site, leading to piperacillin having sub-optimal binding and therefore lowering the activity. Similar observations have been made in the OXA-48-like variant OXA-163 which possesses increased ceftazidime hydrolysis but a lower penicillin activity [63].
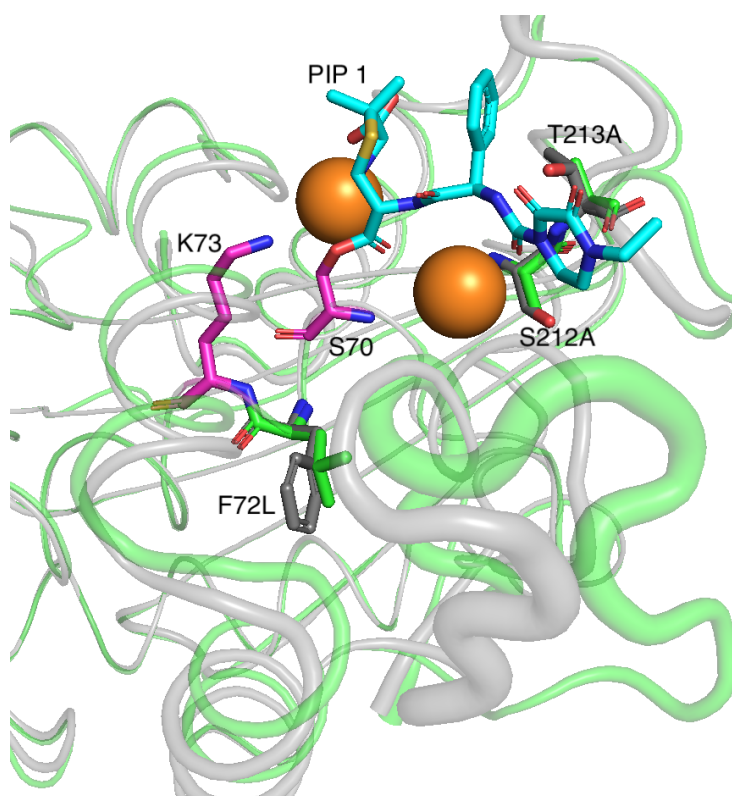
Figure 4A: Shows the active site of OXA-48:Q5 (green) covalently bound to piperacillin aligned with the structure of OXA-48:wt (grey). Piperacillin is shown in cyan, mutations present in the active site is shown as sticks, the chloride ions are shown in orange and the two highly relevant active site residues K72 and S70 is shown in pink. The diameter of the backbone is correlated to the B-factor of the structure. As seen in the structure comparison the Ω-loop is substantially changed.

The decrease in activity against piperacillin and lowering of the melting temperature of OXA-48:Q5 (Table 3C, Figure3E) also points to that a structural change have taken place. Proteins generally keep their fold and overall structure when crystallized due to the large amount of solvent in the crystal [41]. However, packing of the crystal can lead to conformational differences of the surface loops, which is important to keep in mind when comparing crystal structures with different packing, resolution, space group and crystallization conditions. This means that crystal structures may not be completely representative of the enzymes structure in the periplasms. Other methods, such as the ones described in section 4.2 could be used to understand the dynamic implications.

4.3.4 Thermostability and activity trade-offs

Evolving enzymes towards new functionalities through amino acid changes have been described to have trade-offs when gaining resistance towards other substrates, including loss of thermostability and less activity towards the original substrate [64]. Therefore, it was interesting to investigate if OXA-48:F72L and OXA-48:Q5 gained resistance of ceftazidime had any trade-offs. How the intramolecular interactions change in the evolved mutants of OXA-48 towards increased ceftazidime resistance was investigated with kinetics in the presence of urea and DSF.

The melting curves of the enzymes in the presence 6 and 8 M urea did not cover the whole unfolding curve of the proteins, and the results must therefore be interpreted with precaution (Table 3C). At the starting temperature of 20°C the proteins had already partially unfolded with such a high concentration of the chemical denaturant. This can possibly be solved by lowering the starting temperature of the measurements or reducing the time between adding the urea and starting the experiment.

Kinetic experiments also show that the enzymes activity at a concentration of 6 and 8 M urea is very low, leaving the enzyme inactive, likely because the proteins are partially or completely unfolded, as seen from the low or undetermined melting temperatures (Table 3C).

OXA-48:Q5 showed a steeper decline in melting temperature as the concentration of urea increases (Figure 3E) than OXA-48:F72L, indicating that OXA-48:Q5 is less thermostable than OXA-48:F72L. However, both OXA-48:F72L and OXA-48:Q5 have a steeper decline than OXA-48:wt, which indicate that the two mutants display a greater loss in thermostability in the presence of increasing amounts of urea than the wt. The confidence intervals for the slopes of the melting temperatures plotted against the concentrations of urea do not overlap, which indicates that there is a clear difference in the urea dependence on thermostability between OXA-48:wt and the two mutants. This may indicate that OXA-48:F72L and OXA-48:Q5 are more flexible than OXA-48:wt, which in the altered solvent environment created by urea makes the mutants more readily solvated than the wt, leading to the proteins being more readily unfolded [54]. There does not seem to be an additive effect on thermostability as the two mutants have comparable decrease in thermostability compared to the wt even though OXA-48:Q5 (A33V/K51E/F72L/S212A/T213A) has four additional mutations to OXA-48:F72L, which is in line with previous studies [65].

Studying the shape and curvature of the melting curves supplied in Appendix A4, OXA-48:wt without urea present is observed to unfold in a single process, which indicates that the protein has no hydrophobic regions the dye can bind to until an estimate of 45°C, whereas the two mutants seem have a two-step process for the unfolding with no urea present, with a small and a bigger peak during unfolding. This indicates that there are hydrophobic residues available before the unfolding process has fully begun, which indicates that the mutants are more flexible than the wt, exposing hydrophobic residues within the enzyme. For 2 M and up to 8 M urea present the melting curves have similar patterns for all three proteins.

The enzyme activity of OXA-48:wt is less affected by 1 M urea than the two mutants, decreasing by only 10%, whereas the two mutants decrease by 75% and 60% respectively for OXA-48:F72L and OXA-48:Q5. OXA-48:F72L showed a 66% and OXA-48:Q5 a 53% decrease in activity from 0 M urea to 2 M urea present in the solution during kinetic experiments. At 4 M OXA-48:F72L can be considered inactive, whereas OXA-48:wt and OXA-48:Q5 retain an activity of 35%. For OXA-48:wt no standard deviation was obtained since the experiment was performed only one time at each urea concentration, thus the experiment should be repeated. Still the results are comparable to those of the DFS measurements and are still included in the analysis. Melting curves were not obtained for 1 M urea and should also be included in further experiments.

5 Conclusions

In this work, the previously evolved single mutant OXA-48:F72L and the variant OXA-48:Q5 evolved towards increased ceftazidime were studied. The main goals of the work were to understand the catalytic relevance of amino acid substitutions acquired during evolution towards ceftazidime resistance, and to investigate any trade-offs including penicillinase activity and thermostability. Structural studies were also done in order to gain insight intro substrate binding in OXA-48:Q5, to shed light on whether the acquired mutations imposed structural changes that were responsible for the functional trade-offs.

The OXA-48 variants were found to have a pH-dependency, where the catalytic efficiency k_{cat}/K_M for OXA-48:wt showed a 4-fold decrease in activity at pH 5.2 compared to pH 7.2. OXA-48:F72L showed a 5-fold decrease, and OXA-48:Q5 showed a 3-fold decrease in activity at pH 5.2 relative to pH 7.2.

Steady-state enzyme kinetics revealed that the two evolved variants do indeed show increased catalytic activity against ceftazidime compared to OXA-48:wt. OXA-48:F72L revealed a 35-fold increase in the catalytic efficiency k_{cat}/K_m, and OXA-48:Q5 a 32-fold increase relative to OXA-48:wt. The structural hypothesis of the increased ceftazidime resistance in OXA-48:Q5 was increased flexibility within the Ω-loop, which may aid in the binding of the bulkier substrate ceftazidime. However, the conformational change observed was elusive, and alternative methods would need to be applied to further investigate this hypothesis.

Increased ceftazidime resistance in OXA-48:F72L and OXA-48:Q5 showed a trade-off in penicillinase activity. Steady-state enzyme kinetic showed that the catalytic efficiency of both evolved variants had a decrease in piperacillin activity compared to OXA-48:wt, with OXA-48:F72L having a 117-fold decrease and OXA-48:Q5 having a 12-fold decrease in catalytic efficiency compared to OXA-48:wt, respectively. The structural hypothesis for this trade-off was an expansion of the active site, supported by presented OXA-48:Q5 structure with piperacillin where two chloride ions are in the active site, leading to piperacillin having sub-optimal binding.

The OXA-48 variants also displayed a thermostability trade-off, with OXA-48:F72L and OXA-48:Q5 displaying a similar decrease in melting temperature, which indicates that the trade-off is not additive.

In the presence of urea, OXA-48:F72L and OXA-48:Q5 had similar urea dependent melting temperatures, displaying a greater loss in thermostability in the presence of increasing amounts of urea compared to OXA-48:wt. However, OXA-48:F72L displayed a greater urea dependence on enzyme activity, being considered inactive at 4 M urea, whereas OXA-48:wt and OXA-48:Q5 were not considered inactive until 6 M urea.

6 Future work

A natural continuation of this thesis would be to analyze the structure obtained from the crystal of OXA-48:F72L and continuing the crystallization and X-ray crystallography work by further optimizing the crystallization conditions, growing more crystals, and studying the resulting structures, including in complex with more substrates. In addition, attempting to crystallize OXA-48:wt and OXA-48:Q5 in complex with ceftazidime to gain structural insight into these would be a natural step. Co-crystallization or the use of inactive mutants of OXA-48:wt could possibly be used to obtain desired crystal structures of the enzyme in complex with different substrates.

Steady-state enzyme kinetics with the substrate ceftazidime at lower and higher pHs to investigate the pH dependency of the enzyme would also be interesting to implement as a part of the study.

However, these methods have limitations, as previously discussed, and will not provide the whole picture, and other methods such as NMR and molecular dynamic simulations would need to be used to understand the dynamical implications of the mutations.

References

1.   WHO. *Antimicrobial resistance: global report on surveillance.* Summary report published as technical document with reference number: WHO/HSE/PED/AIP/2014.2, (2014).

2.   O'Neill, J., *Tackling Drug-Resistant Infections Globally: Final Report and Recommendations*, Access: https://amr-review.org/Publications.html., Access date: 30.08.2021. (2014).

3.   Bush, K. and Bradford, P. A. *β-Lactams and β-Lactamase Inhibitors: An Overview.* Cold Spring Harb Perspect Med, doi:10.1101/cshperspect.a025247, **6**, (2016).

4.   Aslam, B., Wang, W., Arshad, M. I., Khurshid, M., Muzammil, S., Rasool, M. H. et al., *Antibiotic resistance: a rundown of a global crisis.* Infect Drug Resist, **11**: p. 1645-1658, doi:10.2147/IDR.S173867 (2018).

5.   Dabos, L., Zavala, A., Bonnin, R.A., Beckstein, O., Retailleau, P., Iorga, B. I. and Naas, T., *Substrate Specificity of OXA-48 after β5-β6 Loop Replacement.* ACS Infect Dis, **6**, p. 1032-1043, doi:10.1021/acsinfecdis.9b00452 (2020).

6.   Poirel, L., Naas, T. and Nordmann, P, *Diversity, epidemiology, and genetics of class D β-lactamases.* Antimicrob Agents Chemother, **54**: p. 24-38, doi:10.1128/AAC.01512-08 (2010).

7.   Pitout, J.D.D., Peirano, G., Kock, M. M., Strydom, K. A. and Matsumura, Y., *The Global Ascendency of OXA-48-Type Carbapenemases.* Clin Microbiol Rev, 2019. **33**, doi:10.1128/CMR.00102-19 (2019).

8.   Frohlich, C., Gama, J. A., Harms, K., Hirvonen, V. H. A., Lund, B. A., van der Kamp, M. W. et al., *Cryptic β-Lactamase Evolution Is Driven by Low β-Lactam Concentrations.* mSphere, **6**, doi:10.1128/mSphere.00108-21 (2021).

9.   Frohlich, C., Sorum, V., Thomassen, A. M., Johnsen, P. J., Leiros, H. S. and Samuelsen, O., *OXA-48-Mediated Ceftazidime-Avibactam Resistance Is Associated with Evolutionary Trade-Offs.* mSphere, **4**, doi: 10.1128/mSphere.00024-19 (2019).

10.   Dortet, L., Oueslati, S., Jeannot, K., Tande, D., Naas, T. and Nordmann, P., *Genetic and biochemical characterization of OXA-405, an OXA-48-type extended-spectrum β-lactamase without significant carbapenemase activity.* Antimicrob Agents Chemother, **59**: p. 3823-8, doi: 10.1128/AAC.05058-14 (2015).

11.   King D.T., Sobhanifar, S. and Strynadka N.C.J., *The Mechanisms of Resistance to β-Lactam Antibiotics*, in Gotte, M., Matlashewski, G., Wainberg, M., Sheppard, D. (eds) *Handbook of Antimicrobial Resistance*, Springer, New York, NY, p. 177-202, doi:10.1007/978-1-4939-0667-3_10-1 (2014).

12. Sykes, R.B., Bonner, D. P., Bush, K. and Georgopapadakou, N. H., *Azthreonam (SQ 26,776), a synthetic monobactam specifically active against aerobic gram-negative bacteria.* Antimicrob Agents Chemother, **21**, p. 85-92. doi: 10.1128/AAC.21.1.85 (1982).

13. Wilke, M.S., Lovering, A. L. and Strynadka, N. C., *β-lactam antibiotic resistance: a current structural perspective.* Curr Opin Microbiol, **8**, p. 525-33, doi: 10.1016/j.mib.2005.08.016 (2005).

14. Michelow, I.C., McCracken, G. H., *Antibacterial therapeutic agents,* in Cherry, J., Harrison, G. J. D., Kaplan, S. L, Steinbach, W. J. and Hotez, P. (eds), *Textbook of Pediatric Infectious Diseases*, Saunders, p. 3178-3227, (2009).

15. National Institute of Diabetes and Digestive and Kidney Diseases, *Penicillins (4th Generation)* in *LiverTox: Clinical and Research Information on Drug-Induced Liver Injury*. PMID: 31643176. Access date: 15.05.2022. (2012).

16. Bush, K. and Jacoby, G. A., *Updated functional classification of β-lactamases.* Antimicrob Agents Chemother, **54**: p. 969-76, doi: 10.1128/AAC.01009-09 (2010).

17. Sawa, T., Kooguchi, K. and Moriyama, K., *Molecular diversity of extended-spectrum β-lactamases and carbapenemases, and antimicrobial resistance.* J Intensive Care, **8**, doi: 10.1186/s40560-020-0429-6 (2020).

18. Docquier, J. D., Calderone, V., De Luca, F., Benvenuti, M., Giuliani, L. and Bellucci, L. et al., *Crystal structure of the OXA-48 β-lactamase reveals mechanistic diversity among class D carbapenemases.* Chem Biol, **16**: p. 540-547, doi: 10.1016/j.chembiol.2009.04.010 (2009).

19. Poirel, L., Heritier, C., Tolun, V. and Nordmann, P., *Emergence of oxacillinase-mediated resistance to imipenem in Klebsiella pneumoniae.* Antimicrob Agents Chemother, **48**, p. 15-22, doi:10.1128/AAC.48.1.15-22.2004 (2004).

20. Poirel, L., Potron, A., and Nordmann, P., *OXA-48-like carbapenemases: the phantom menace.* J Antimicrob Chemother, **67**, p. 1597-606, doi:10.1093/jac/dks121 (2012).

21. Schneider, K.D., Bethel, C. R., Distler, A. M., Hujer, A. M., Bonomo, A. and Leopnard, D. A., *Mutation of the active site carboxy-lysine (K70) of OXA-1 β-lactamase results in a deacylation-deficient enzyme.* Biochemistry, **48**, p. 6136-45. doi:10.1021/bi900448u (2009).

22. Li, J., Cross, J. B., Vreven, T., Meroueh, S. O., Mobashery, S. and Schlegel, H. B., *Lysine carboxylation in proteins: OXA-10 β-lactamase.* Proteins, **61**, p. 246-57, doi:10.1002/prot.20596 (2005).

23. Hirvonen, V. H. A., Spencer, J. and van der Kamp, M. W., *Antimicrobial Resistance Conferred by OXA-48 β-Lactamases: Towards a Detailed Mechanistic Understanding.* Antimicrob Agents Chemother, **65**, doi: 10.1128/AAC.00184-21 (2021).

24. Campbell, M. K. and Farrell, S., *The behavior of Proteins: Enzymes* In *Biochemistry*. Sixth ed., Brooks/Cole,CA, USA, p. 143-152,(2008).

25. Creighton, T. E., *Proteins: Structures and Molecular Properties*. Second ed. 1993, New York, W. H. Freeman and Company (1993).

26. Petsko, G.A. and Ringe, D., *Protein structure and function*. Primers in biology, Oxford University Press, Sunderland, MA, p.195 (2004).

27. Hirte, K., Seiwert, B., Schuurmann, G. and Reemtsma, T., *New hydrolysis products of the β-lactam antibiotic amoxicillin, their pH-dependent formation and search in municipal wastewater.* Water Res, **88**, p. 880-888, doi:10.1016/j.watres.2015.11.028 (2016).

28. Holdgate, G. A., Meek, T. D. and Grimley, R. I., *Mechanistic enzymology in drug discovery: a fresh perspective.* Nat Rev Drug Discov, **17**, p. 78, doi:10.1038/nrd.2017.257 (2018).

29. Srinivasan, B., *A guide to the Michaelis-Menten equation: steady state and beyond.* FEBS J, doi: 10.1111/febs.16124 (2021).

30. Palzkill, T., *Structural and Mechanistic Basis for Extended-Spectrum Drug-Resistance Mutations in Altering the Specificity of TEM, CTX-M, and KPC β-lactamases.* Front Mol Biosci, **5**, doi: 10.3389/fmolb.2018.00016 (2018).

31. Davidson, V. L. and Sittman, D. B., *biochemistry*. Third ed. The National medical series for independent study, Harwal Publishing, p. 59-62 (1994).

32. Khersonsky, O. and Tawfik, D. S, *Enzyme promiscuity: a mechanistic and evolutionary perspective.* Annu Rev Biochem, **79**, p. 471-505, doi: 10.1146/annurev-biochem-030409-143718 (2010).

33. Walsh, R., *Alternative Perspectives of Enzyme Kinetic Modeling*, in Ekinci, D., *Medicinal Chemistry and Drug Design,* InTech, p. 357-371, doi: 10.5772/36973 (2012).

34. Ericsson, U.B., Hallberg, B. M., Detitta, G. T., Dekker, N. and Nordlund, P., *Thermofluor-based high-throughput stability optimization of proteins for structural studies.* Anal Biochem, **357**, p. 289-98. doi:10.1016/j.ab.2006.07.027 (2006).

35. Vedadi, M., Niesen, F. H., Allali-Hassani, A., Fedorov, O. Y., Finerty, J., Wasney, G. A. Jr. et al., *Chemical screening methods to identify ligands that promote protein stability, protein crystallization, and structure determination.* Proc Natl Acad Sci U S A, **103**, p. 15835-40, doi: 10.1073/pnas.0605224103 (2006).

36. Niesen, F.H., Berglund, H. and Vedadi, M., *The use of differential scanning fluorimetry to detect ligand interactions that promote protein stability.* Nat Protoc, (9), p. 2212-21, doi:10.1038/nprot.2007.321 (2007).

37. Senisterra, G. A. and Finerty, P. J. Jr., *High throughput methods of assessing protein stability and aggregation.* Mol Biosyst, **5**, p. 217-23, doi: 10.1039/b814377c (2009).

38. Berman, H. M., Westbrook, J., Feng, Z., Gilliland, G., Bhat, T. N., Weissig, H., Shindyalov, I. N. and Bourne, P. E., *The Protein Data Bank,* Nucleic Acids Research, **28**, p. 235-242, doi:10.1093/nar/28.1.235 (2000).

39. Committe on Research Opportunities in Biology, Board on Biology and National Research Council, *Molecular Structure and Function* in *Opportunities in Biology* 1989, National Academies Press, Washington DC, p. 39-75 (1989).

40. Adams, P.D., Afonine, P. V., Grosse-Kunstleve, R. W., Read, R. J., Richardson, J. S., Richardson, D. C. et al., *Recent developments in phasing and structure refinement for macromolecular crystallography.* Curr Opin Struct Biol, **19**, p. 566-72, doi: 10.1016/j.sbi.2009.07.014 (2009).

41. McPherson, A. and Gavira, J. A., *Introduction to protein crystallization.* Acta Crystallogr F Struct Biol Commun, **70**, p. 2-20 (2014).

42. Smyth, M. S. and Martin, J. H., *x ray crystallography.* Mol Pathol, **53**, p. 8-14, doi. 10.1136/mp.53.1.8 (2000).

43. Unge, T., *Crystallization Methods*, in Bergfors, T. M., *Protein Crystallization - Techniques, Strategies and tips*, International University Line La Jolla, CA, p.7-11 (1999).

44. Pichlo, C., Montada, A. A., Schacherl, M. and Baumann, U., *Production, Crystallization and Structure Determination of C. difficile PPEP-1 via Microseeding and Zinc-SAD.* J Vis Exp, **188**, doi:10.3791/55022 (2016).

45. Dessau, M.A. and Modis, Y., *Protein crystallization for X-ray crystallography.* J Vis Exp, **47**, doi:10.3791/2285 (2011).

46. Weichenberger, C.X., Afonine, P. V., Kantardjieff, K. and Rupp, B., *The solvent component of macromolecular crystals.* Acta Crystallogr D Biol Crystallogr, **71**, p. 1023-38, doi:10.1107/S1399004715006045 (2015).

47. Leonard, D.A., Bonomo, R. A. and Powers, R. A., *Class D β-lactamases: a reappraisal after five decades.* Acc Chem Res, **46**, p. 2407-15, doi: 10.1021/ar300327a (2013).

48. Gasteiger, E., Hoogland, C., Gattiker, A., Duvaud, S., Wilkins, M. R., Appel, R. D. and Bairoch, A., *Protein Identification and Analysis Tools on the ExPASy Server*, in Walker, J. M., *The Proteomics Protocols Handbook*, Humana Press, p. 571-607 (2005).

49. Nesheim, B. H. B., *Characterization and structural analysis of class D β-lactamases: variants and mutants of OXA-type carbapenemases* in *Chemistry,* UiT, Arctic University of Norway, Munin (2016).

50. McCoy, A.J., Grosse-Kunstleve, R. W, Adams, P. D., Winn, M. D., Storoni, L. C. and Read, R. J., *Phaser crystallographic software.* J Appl Crystallogr, **40**, p. 658-674, doi: 10.1107/S0021889807021206 (2007).

51. *The PyMOL Molecular Graphics System*. Schrödinger, LLC.

52. Laskowski, R. A and Swindells, M. B., *LigPlot+: multiple ligand-protein interaction diagrams for drug discovery.* J. Chem. Inf. Model., **51**, p. 2778-2786, doi:10.1021/ci200227u (2011).

53. Kumar, G., Issa, B., Kar, D., Biswal, S. and Ghosh, A. S., *E152A substitution drastically affects NDM-5 activity.* FEMS Microbiol Lett, **364**, doi:10.1093/femsle/fnx008 (2017).

54. Bennion, B.J. and Daggett, V., *The molecular basis for the chemical denaturation of proteins by urea.* Proc Natl Acad Sci USA, **100,** p. 5142-7, doi: 10.1073/pnas.0930122100 (2003).

55. Zhou, R, Li, J., Hua, L., Yang, Z and Berne, B. J., *Comment on "Urea-Mediated Protein Denaturation: A Consensus View".* J. Phys. Chem, **115**, p. 1323-1326, doi: 10.1021/jp105160a (2011).

56. Abuin, E.B., Lissi, E. A., Aspee, A., Gonzales, F. D. and Varas, J. M., *Fluorescence of 8-Anilinonaphthalene-1-sulfonate and Properties of Sodium Dodecyl Sulfate Micelles in Water-Urea Mixtures.* J Colloid Interface Sci, **186**, p. 332-8, doi: 10.1006/jcis.1996.4648 (1997).

57. Strokach, A., Corbi-Verge, C., Teyra, J. and Kim, P. M., *Predicting the Effect of Mutations on Protein Folding and Protein-Protein Interactions.* Methods Mol Biol, **1851**, p. 1-17, doi:10.1007/978-1-4939-8736-8_1 (2019).

58. King, D.T., King, A. M., Lal, S. M., Wright, G. D. and Strynadka, N. C., *Molecular Mechanism of Avibactam-Mediated β-Lactamase Inhibition.* ACS Infect Dis, **1**, p. 175-84, doi:10.1021/acsinfecdis.5b00007 (2015).

59. Szarecka, A., Lesnock, K. R., Ramirez-Mondragon, C. A., Nicholas, H. B. Jr. and Wymore, T., *The Class D β-lactamase family: residues governing the maintenance and diversity of function.* Protein Eng Des Sel, **24**, p. 801-9, doi:10.1093/protein/gzr041 (2011).

60. Yang, G., Miton, C. M. and Tokuriki, N., *A mechanistic view of enzyme evolution.* Protein Sci, **29**, p. 1724-1747, doi:10.1002/pro.3901 (2020).

61. Stojanoski, V., Chow, D. C., Fryszczyn, B., Hlu, L., Nordmann, P., Poirel, L. et al., *Structural Basis for Different Substrate Profiles of Two Closely Related Class D β-Lactamases and Their Inhibition by Halogens.* Biochemistry, **54**, p. 3370-80, doi: 10.1021/acs.biochem.5b00298 (2015).

62. Petrovic, D., Risso, V. A., Kamerlin, S. C. L. and Sanchez-Ruiz, J. M., *Conformational dynamics and enzyme evolution.* J R Soc Interface, **15**, doi: 10.1098/rsif.2018.0330 (2018).

63. Poirel, L., Castanheira, M., Carrer, A., Rodriguez, C. P., Jones, R. N., Smayevsky, J. et al., *OXA-163, an OXA-48-related class D β-lactamase with extended activity toward expanded-spectrum cephalosporins.* Antimicrob Agents Chemother, **55**, p. 2546-51, doi:10.1128/AAC.00022-11 (2011).

64. Thomas, V.L., McReynolds, A. C. and Shoichet, B. K., *Structural bases for stability-function tradeoffs in antibiotic resistance.* J Mol Biol, **396**, p. 47-59, doi: 10.1016/j.jmb.2009.11.005 (2010).

65. Fröhlich, C., *On the Evolvbility of OXA-48: A comprehensive study of new functions within the β-lactamase OXA-48*, in *Chemistry*, Munin, The Arctic University of Norway, Tromsø (2021).
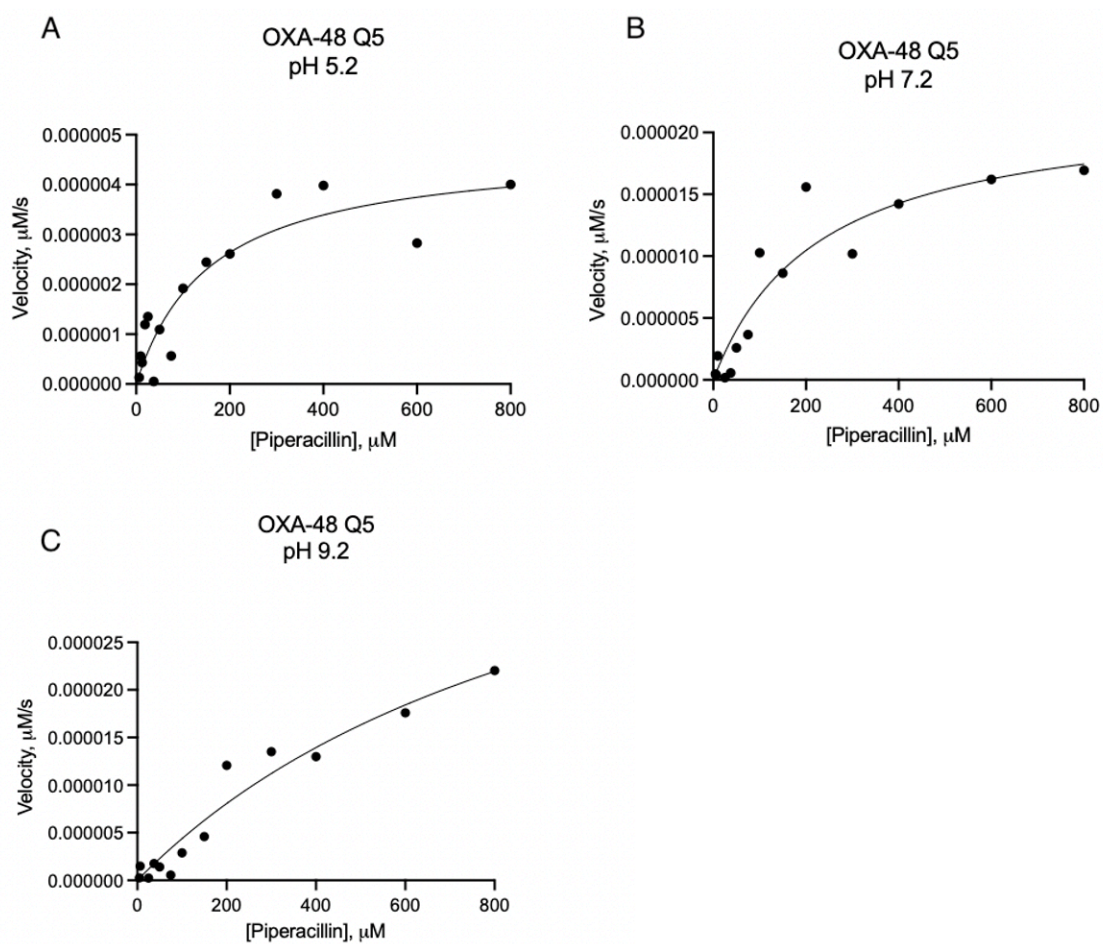
Appendix

Kinetics data
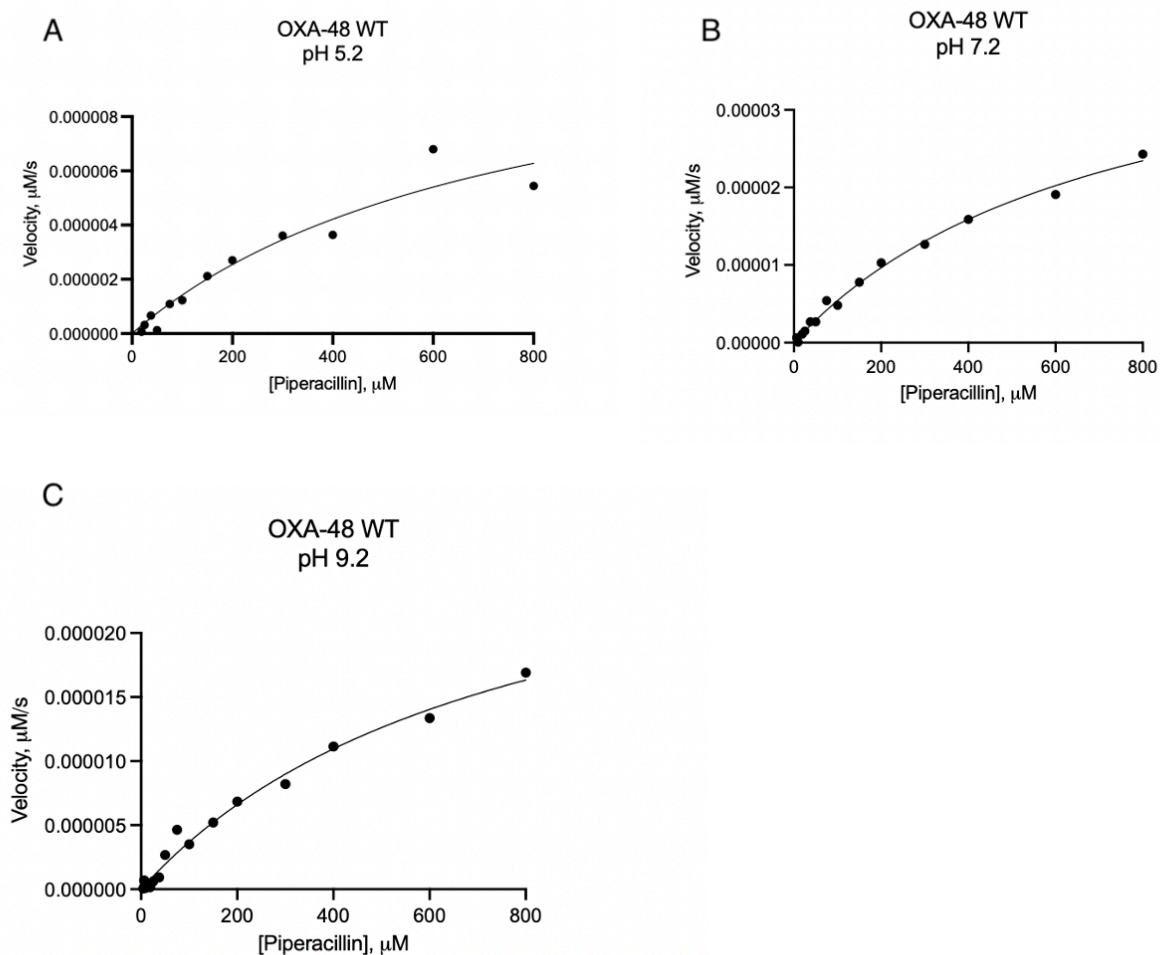
Figure A1: Enzyme kinetics curves for OXA-48:wt at A) pH 5.2 , B) 7.2 and C) 9.2 with the substrate piperacillin. Substrate concentration is on the x-axis and the reaction velocity is on the y-axis.
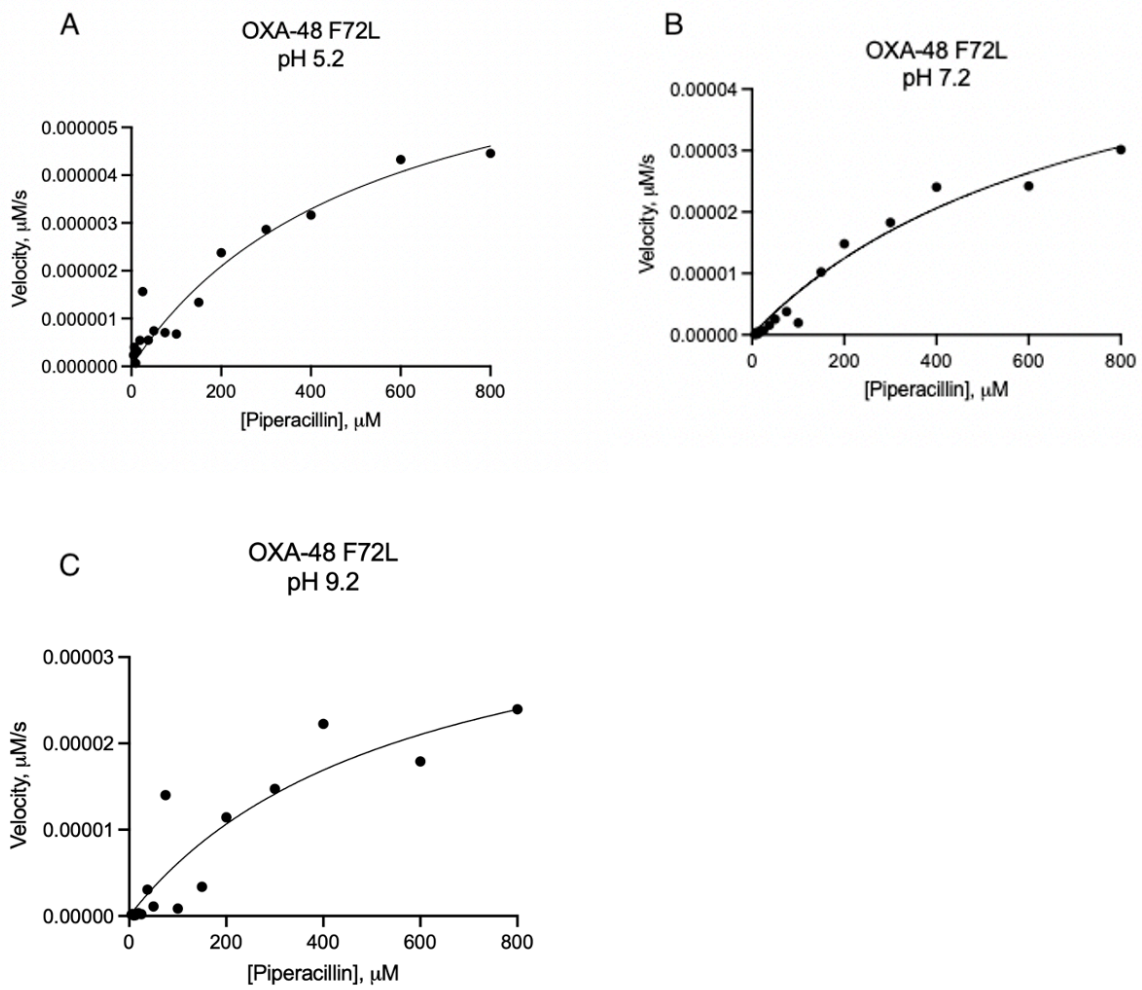
Figure A2: Enzyme kinetics curves for OXA-48:F72L at A) pH 5.2, B) 7.2 and C) 9.2 with the substrate piperacillin. Substrate concentration is on the x-axis and the reaction velocity is on the y-axis.

Figure A3: Enzyme kinetics curves for OXA-48:Q5 at A) pH 5.2, B) 7.2 and C) 9.2 with the substrate piperacillin. Substrate concentration is on the x-axis and the reaction velocity is on the y-axis.
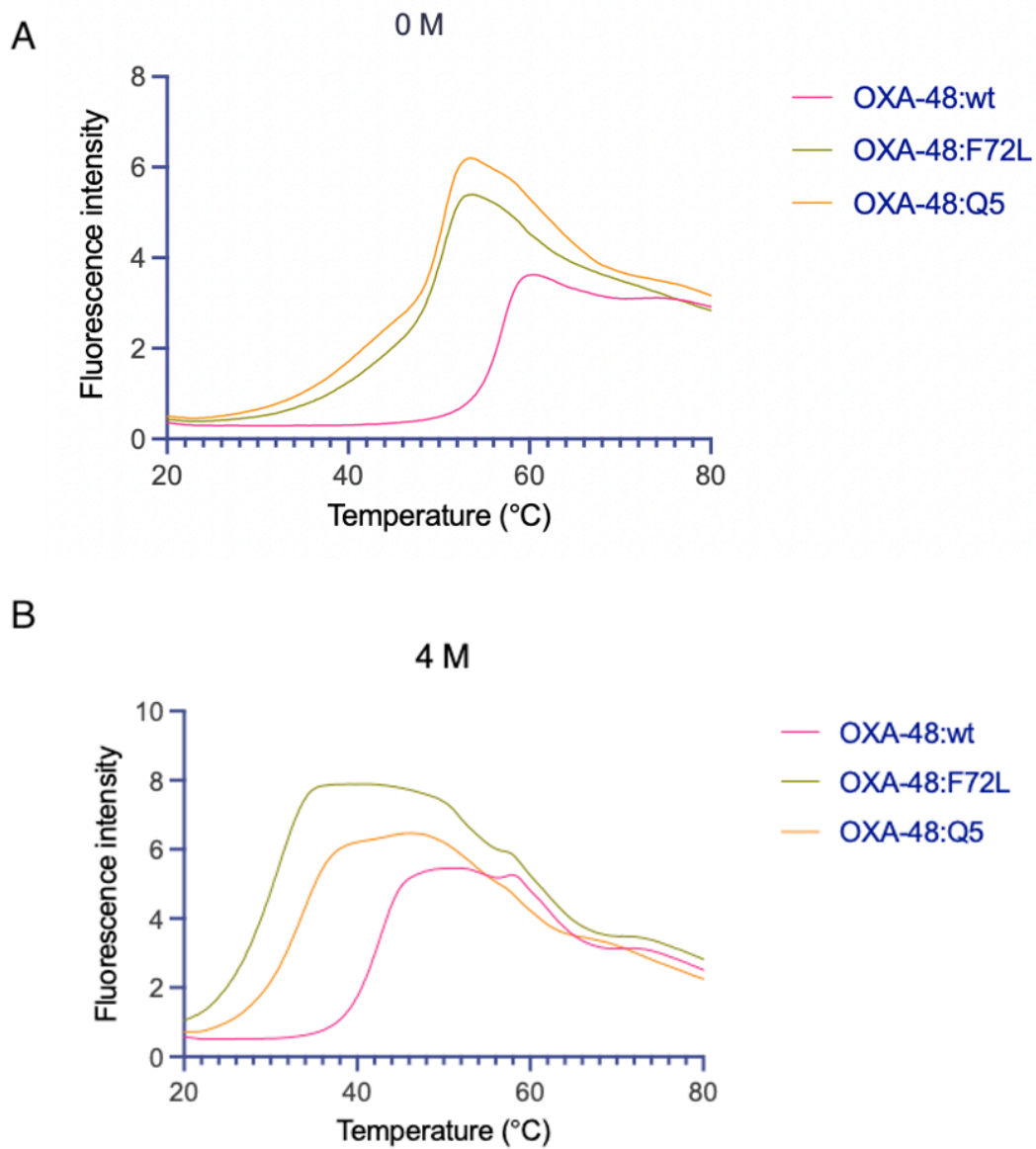
Melting curves

Figure A4: Shows the fluorescence intensity plotted against temperature for the three enzymes OXA-48:wt, OXA-48:F72L and OXA-48:Q5 with A) 0 M urea and B) 4 M urea.

Crystallization data

Table A1: X-ray data collection and refinement statistics for OXA-48:Q5 in complex with piperacillin. Statistics for the highest-resolution shell are shown in parentheses.

Diffraction source	ESRF ID23-EH2
Wavelength	0.8731 Å
Resolution range (Å)	23.00-1.50
	(1.55-1.50)
Space group	C 1 2 1
Unit cell: a,b,c (Å)	91.90, 45.34, 64.33
α,β,γ (°)	90, 107.23, 90
Total reflections	207695 (20379)
Unique reflections	40619 (4030)
Multiplicity	5.1 (5.1)
Completeness (%)	99.80 (99.93)
Mean I/sigma(I)	11.42 (1.97)
Wilson B-factor (Å^2)	16.42
R-merge	0.08011 (0.7382)
R-meas	0.08939 (0.824)
R-pim	0.0389 (0.3597)
$CC_{1/2}$	0.998 (0.684)
CC*	0.999 (0.901)

Resolution (Å)	23.00-1.50 (1.55-1.50)
Reflections used in refinement	40617 (4030)
Reflections used for R-free	1995 (198)
R-work	0.1583 (0.2622)
R-free	0.1954 (0.2826)
CC(work)	0.974 (0.836)
CC(free)	0.961 (0.786)
Number of non-hydrogen atoms	2609
Macromolecules	2251
Ligands	15
Solvent	343
Protein residues	242
RMS(bonds) (Å)	0.021
RMS(angles) (°)	97.08
Ramachandran favored (%)	2.08
Ramachandran allowed (%)	0.83
Ramachandran outliers	2.61
Clashscore	11.89
Average B-factor (Å^2)	24.55
Macromolecules (Å^2)	22.04
Ligands (Å^2)	45.15
Solvent (Å^2)	20.15
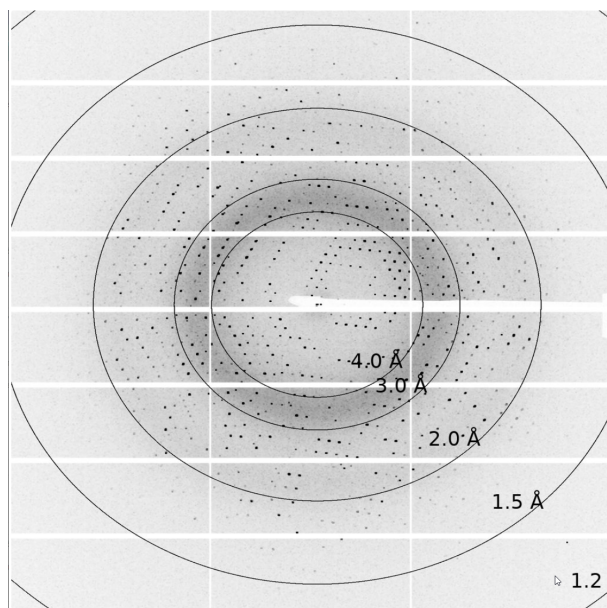
Figure A5: Diffraction image of OXA-48:Q5 soaked with piperacillin, where the resolution circles are depicted and labelled. This image is part of the complex structure presented in Table A1. See the results for more details.

Interactions within the OXA-48:Q5 in complex with piperacillin structure

Table A2: Shows distances and type of interaction for PIP1 in the active site of OXA-48:Q5 in complex with piperacillin. Residues given with two distances have two bonds to the residue given.

Residue 1 in interaction	Residue 2 in interaction	Type of interaction	Bond length (Å)
PIP 1	S70	Covalent bond	1.4
PIP 1	S70	Hydrogen bond	2.74
PIP 1	Y211	Hydrogen bond	2.82, 2.92
PIP 1	A213	Hydrogen bond	3.1
PIP 1	Cl$^-$ 2	Hydrogen bond	2.59, 3.08
Cl$^-$ 2	T209	Hydrogen bond	2.84
Cl$^-$ 2	R250	Hydrogen bond	3.12
Cl$^-$ 3	PIP 1	Hydrogen bond	2.64

Table A3: Shows distances and type of interaction for PIP2 in OXA-48:Q5 in complex with piperacillin. Residues given with several distances have several bonds to the residue given.

Residue 1 in interaction	Residue 2 in interaction	Type of interaction	Bond length (Å)
PIP 2	K39	Hydrogen bond	3.07
PIP 2	H38	Hydrogen bond	2.89, 3.18, 2.63